Distinct signaling mechanisms regulate migration in unconfined versus confined spaces

Wei-Chien Hung,[1,3] Shih-Hsun Chen,[1,2] Colin D. Paul,[1,2,4] Kimberly M. Stroka,[1,2,4] Ying-Chun Lo,[5] Joy T. Yang,[6] and Konstantinos Konstantopoulos[1,2,3,4,5]

[1]Department of Chemical and Biomolecular Engineering; [2]Physical Sciences-Oncology Center; [3]Center for Cancer Nanotechnology Excellence; [4]Institute for NanoBioTechnology; and [5]Department of Oncology and [6]Department of Cell Biology, School of Medicine; Johns Hopkins University, Baltimore, MD 21218

Using a microchannel assay, we demonstrate that cells adopt distinct signaling strategies to modulate cell migration in different physical microenvironments. We studied α4β1 integrin–mediated signaling, which regulates cell migration pertinent to embryonic development, leukocyte trafficking, and melanoma invasion. We show that α4β1 integrin promotes cell migration through both unconfined and confined spaces. However, unlike unconfined (2D) migration, which depends on enhanced Rac1 activity achieved by preventing α4/paxillin binding, confined migration requires myosin II–driven contractility, which is increased when Rac1 is inhibited by α4/paxillin binding. This Rac1–myosin II cross talk mechanism also controls migration of fibroblast-like cells lacking α4β1 integrin, in which Rac1 and myosin II modulate unconfined and confined migration, respectively. We further demonstrate the distinct roles of myosin II isoforms, MIIA and MIIB, which are primarily required for confined and unconfined migration, respectively. This work provides a paradigm for the plasticity of cells migrating through different physical microenvironments.

Introduction

Integrins regulate cell migration by transducing signals bidirectionally across the plasma membrane. Integrin signaling is mediated by the interactions between the cytoplasmic domains of integrins and signaling proteins, which form multimolecular complexes via adaptor proteins. The role of integrin signaling in regulating cell migration is exemplified by an α4β1 integrin–mediated pathway (Nishiya et al., 2005). α4β1 integrin binds to the CS-1 region of fibronectin, an ECM protein, and to VCAM-1 (vascular cell adhesion molecule 1), which is expressed on activated endothelium. Engagement of α4β1 integrin to fibronectin plays a critical role in cell migration during embryonic development (Kil et al., 1998; Sengbusch et al., 2002; Grazioli et al., 2006), whereas engagement to VCAM-1 facilitates leukocyte trafficking (Berlin et al., 1995; Konstantopoulos and McIntire, 1997) and tumor angiogenesis (Garmy-Susini et al., 2005). α4β1 integrin is also implicated in melanoma metastasis. Notably, α4 integrin is one of the top hits in a genome-wide expression profiling study for genes that are up-regulated in invasive compared with noninvasive melanoma (Ryu et al., 2007).

Using a CHO cell model, it was demonstrated that α4β1 integrin promotes lamellipodia protrusion and directionally persistent cell migration, which are regulated by molecular interactions at the cytoplasmic tail of the α4 integrin subunit (α4 tail; Goldfinger et al., 2003; Lim et al., 2007; Rivera Rosado et al., 2011). The best studied interaction at the α4 tail involves its binding to paxillin (Liu et al., 1999), which forms an α4/paxillin/GIT1 complex that inhibits Rac1 activation (Nishiya et al., 2005). α4/paxillin binding is negatively regulated by PKA-dependent phosphorylation of Ser988 in the α4 tail (Ser^{988} phosphorylation; Han et al., 2001). α4β1 integrin–dependent cell migration on a 2D substratum is suppressed when Ser^{988} phosphorylation is disrupted by substitution of Ser988 with Ala (S988A mutation) but enhanced when α4/paxillin binding is disrupted by substitution of Tyr991 with Ala (Y991A mutation). α4/paxillin binding and Ser^{988} phosphorylation differentially modulate Rac1 activation, thus regulating lamellipodia protrusion and directionally persistent cell migration on a 2D surface

Correspondence to Konstantinos Konstantopoulos: konstant@jhu.edu; or Joy T. Yang: jyang@jhmi.edu

Abbreviations used in this paper: MLCK, myosin light chain kinase; PAK, p21-activated kinase; PBD, p21-binding domain; PDMS, polydimethylsiloxane; ROCK, RhoA-associated protein kinase; TIRF, total internal reflection fluorescence, WT; wild type.

The Rockefeller University Press $30.00
J. Cell Biol. Vol. 202 No. 5 807–824
www.jcb.org/cgi/doi/10.1083/jcb.201302132

(Goldfinger et al., 2003; Nishiya et al., 2005). However, it is not known how the molecular interactions at the α4 tail regulate cell migration through physically confined, as opposed to unconfined (2D), microenvironments encountered in vivo.

Cells migrate in vivo within 3D ECMs. Cells also migrate through 3D longitudinal tracks with bordering 2D interfaces (i.e., channels). These channels are formed between the connective tissue and the basement membrane of muscle, nerve, and epithelium (Friedl and Alexander, 2011). 3D longitudinal channels are also formed between adjacent bundled collagen fibers in fibrillar interstitial tissues (Friedl and Alexander, 2011). Importantly, cells have been reported to migrate through such 3D channels in vivo (Alexander et al., 2008). The cross-sectional areas (Wolf et al., 2009) of pores/channels encountered an in vivo range from 10 to >400 μm^2. Consequently, cells migrating in vivo experience varying degrees of physical confinement. Accumulating evidence suggests that physical confinement alters cell migration mechanisms (Balzer et al., 2012; Pathak and Kumar, 2012; Konstantopoulos et al., 2013). To address how α4 tail–mediated signaling regulates cell migration in physically confined microenvironments, we used a microchannel device (Balzer et al., 2012; Tong et al., 2012a; Chen et al., 2013), which tracks cells migrating through four-walled channels of varying degrees of confinement: from unconfined (2D) migration when the channel width, W, is larger than the cell diameter, d_{cell}, (wide channels) to confined migration when $W < d_{cell}$ (narrow channels). Using this microchannel assay, we herein report that α4 tail–mediated signaling differentially modulates cell migration on 2D versus physically confined microenvironments via negative feedback between Rac1 and myosin II. Through this cross talk mechanism, the migration of fibroblast-like cells, which are devoid of α4β1 integrin, is also controlled by Rac1 and myosin II in 2D and confined spaces, respectively. This work provides a paradigm supporting the view that the physical microenvironment alters the routes within a signaling network to achieve maximal cellular responses.

Results

α4 tail mutations exert distinct effects on wide versus narrow channel migration

To study the effects of α4 cytoplasmic tail interactions on cell migration, we used stable CHO cell lines, which ectopically express the wild-type (WT) α4 integrin (CHO-α4WT) or α4 integrin carrying specific cytoplasmic mutations that disrupt paxillin binding (CHO-α4Y991A) or Ser^{988} phosphorylation (CHO-α4S988A; Pinco et al., 2002; Dikeman et al., 2008). We confirmed that CHO-α4WT, CHO-α4Y991A, and CHO-α4S988A cells express equivalent levels of α4 integrin on their surfaces, as assessed by flow cytometry (Fig. S1). We tested the migratory potential of each cell type in a microchannel assay (Balzer et al., 2012; Tong et al., 2012a; Chen et al., 2013). In this assay, cells migrate toward a chemoattractant source through VCAM-1– or fibronectin-coated, four-walled rectangular channels of fixed length (200 μm) and height (10 μm) but variable width (3, 6, 10, 20, or 50 μm; Fig. 1). Cells migrating through 50-μm-wide channels are not constricted by the polydimethylsiloxane (PDMS) channel walls and protrude lamellipodia similar to those on 2D planar surfaces (Figs. 1 and 2). We evaluated the effect of VCAM-1 concentration on the speed of cell migration (defined as total distance traveled divided by time). As shown in Fig. 2 A, all cell types migrating through 50-μm-wide channels exhibited a biphasic dependence of the migration speed on ligand concentration, with maximum speeds at intermediate VCAM-1 concentrations (1–2 μg/ml corresponding to ∼1,150–2,000 molecules/μm^2, as determined by the Europium assay; Tong et al., 2012b). This pattern is typical of 2D migration (DiMilla et al., 1993). Consistent with a previous study (Goldfinger et al., 2003), CHO-α4S988A cells displayed the lowest migration speed over a wide spectrum of ligand concentrations, whereas CHO-α4Y991A cells had either a similar migration speed with CHO-α4WT cells at low/intermediate VCAM-1 concentrations or moved faster than CHO-α4WT cells at higher ligand concentration (≥5 μg/ml; Fig. 2 A).

As the channel width decreases ($W < 50$ μm), cells progressively experience physical confinement by the lateral channel walls and undergo deformation to squeeze and move through the channels (Fig. 1). Narrow (6 or 3 μm) channels induce cell contact with all four-channel walls and emulate migration through a physically constricted microenvironment (referred to as confined migration; Balzer et al., 2012). In narrow channels, the migration speed of CHO-α4WT cells remained maximal up to intermediate VCAM-1 concentrations (0–2 μg/ml) and progressively decreased at higher concentrations (Fig. 2 A). In contrast to wide (50 μm) channels, CHO-α4Y991A cells exhibited the lowest migration speed over a wide range of VCAM-1 concentrations, whereas CHO-α4S988A migrated as efficiently as CHO-α4WT cells at low/intermediate VCAM-1 concentrations in narrow channels (Fig. 2 A). We also quantified migration persistence by measuring the cell chemotactic index (defined as the ratio of the net displacement to the total distance traveled) and migration velocity (defined as net displacement divided by time). No major differences were noted between migration speed versus velocity because all CHO cell types had persistent cell motility in response to FBS (Figs. 2 A and S2). Because migration velocity represents the overall motile activity of the cells in response to a chemotactic stimulus, this parameter was used in the studies hereafter.

We quantified the migratory velocity of each cell type in response to increasing degrees of confinement using microchannels coated with 1 μg/ml VCAM-1 because this concentration provided near maximal speeds of migration in both wide and narrow channels. CHO-α4WT cells migrated efficiently through channels of different widths with a migration velocity of ∼30 μm/h. CHO-α4Y991A cells displayed progressively reduced cell motility in channels of decreasing width (Fig. 2 B and Video 1). In contrast, the velocity of CHO-α4S988A cells gradually increased with decreasing channel width (Fig. 2 B and Video 1). Similar phenomena were also observed in 5 μg/ml fibronectin-coated microchannels (Fig. 2 C), thereby generalizing our observations to ECM proteins found in confined spaces in vivo. These data reveal the divergent effects of the α4 tail mutations on the migration of α4β1 integrin–expressing CHO cells through wide versus narrow channels. They also suggest that α4β1 integrin may modulate and optimize cell migration via

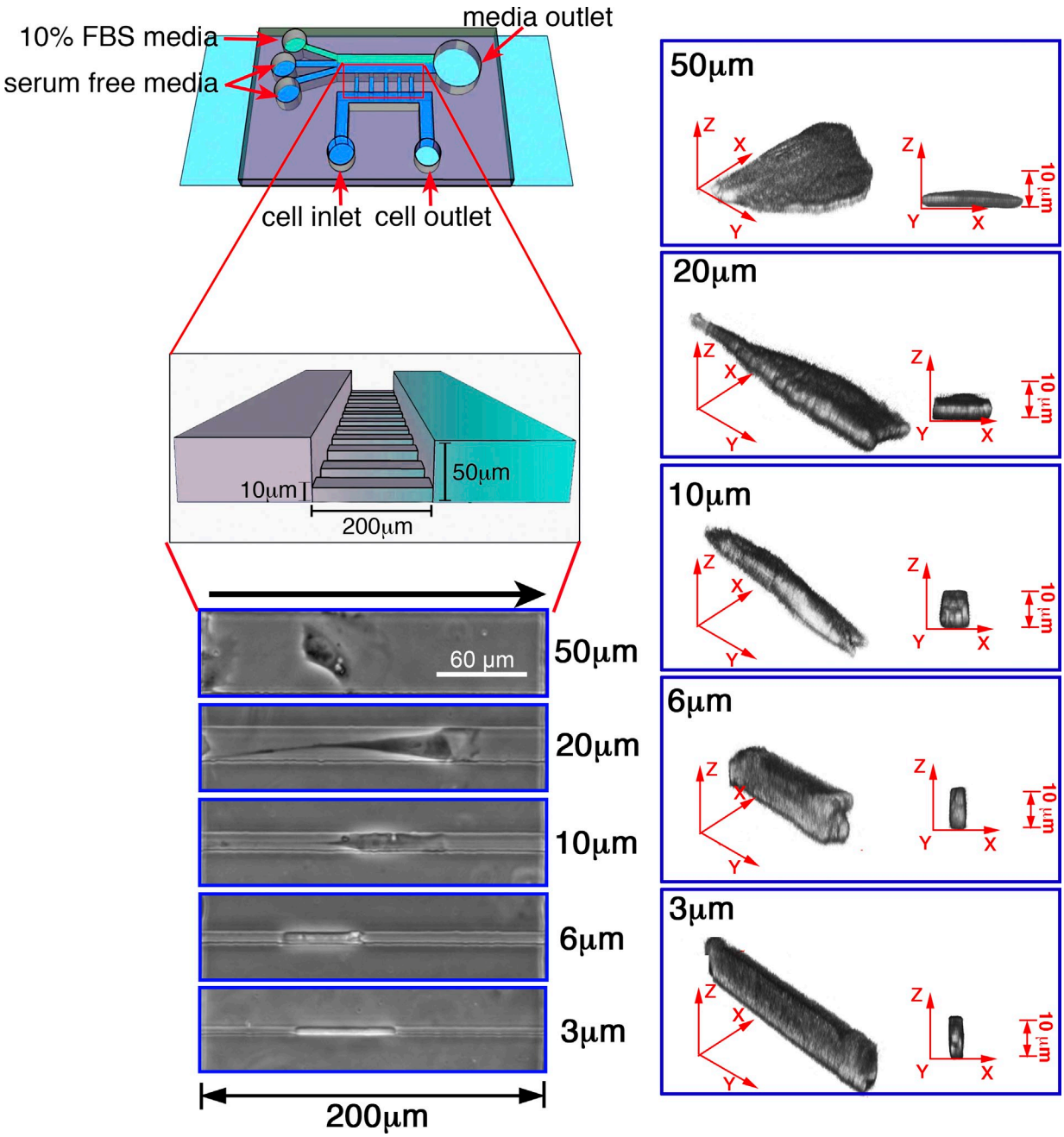

Figure 1. **Overview of the microchannel device.** Schematic of the migration chamber bonded to coverslips (light blue), with inlet ports for serum-free media or cells (dark blue) or FBS (10%; green). Also shown is a close-up detailing the dimensions of the microchannel array, along with phase contrast and 3D reconstruction images of CHO-α4WT cells in microchannels of different widths. The black arrow (above the phase images) indicates the direction of migration.

distinct mechanisms when the cells are subjected to different physical microenvironments.

Inhibition of Rac1 activation and the RhoA–myosin pathway in CHO-α4WT cells recapitulates the migratory phenotypes of CHO-α4S988A and CHO-α4Y991A cells, respectively

The finding that α4/paxillin binding inhibits Rac1 activation (Nishiya et al., 2005) prompted us to investigate the role of Rac1 in cell migration through channels of varying degrees of confinement, using the Rac1-specific small molecule inhibitor NSC23766 (100 μM). CHO-α4WT cells treated with NSC23766 displayed reduced lamellipodial protrusion relative to controls and a markedly suppressed migration velocity through 50-μm-wide channels (Fig. 3 A and Video 2). The inhibitory effect of NSC23766 was progressively diminished with decreasing channel width, and was minimal for the migration of CHO-α4WT cells through 10-, 6-, or 3-μm channels (Fig. 3 A and Video 2). To confirm the specificity of this intervention, we knocked down Rac1 in CHO-α4WT cells via RNAi and examined the migratory potential of Rac1-depleted and scramble control cells

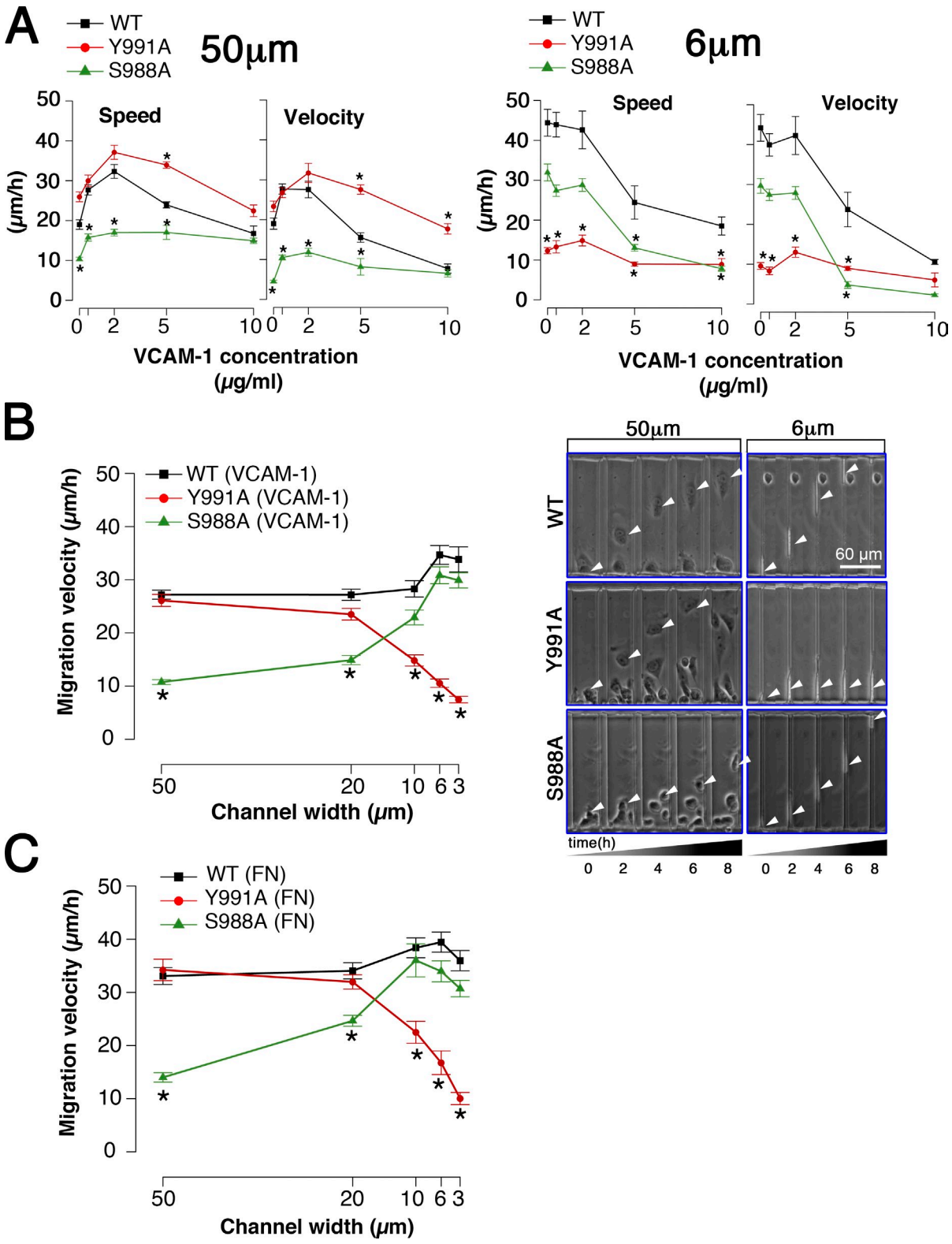

Figure 2. **Effects of the α4 tail mutations on cell migration in microchannels.** (A) The migration speed and velocity of CHO-α4WT, CHO-α4Y991A, and CHO-α4S988A cells through 50- or 6-μm microchannels as a function of VCAM-1–coating concentration. Data represent means ± SEM of >20 cells from three independent experiments. (B and C) The influence of channel width on cell migration velocity through microchannels coated with 1 μg/ml VCAM-1 (B) or 5 μg/ml fibronectin (FN; C). Data represent means ± SEM of >30 cells from three independent experiments. In B, the images of migrating cells in designated channel widths and time points are also shown. White arrowheads show the centroid of cell body. *, $P < 0.005$ relative to CHO-α4WT.

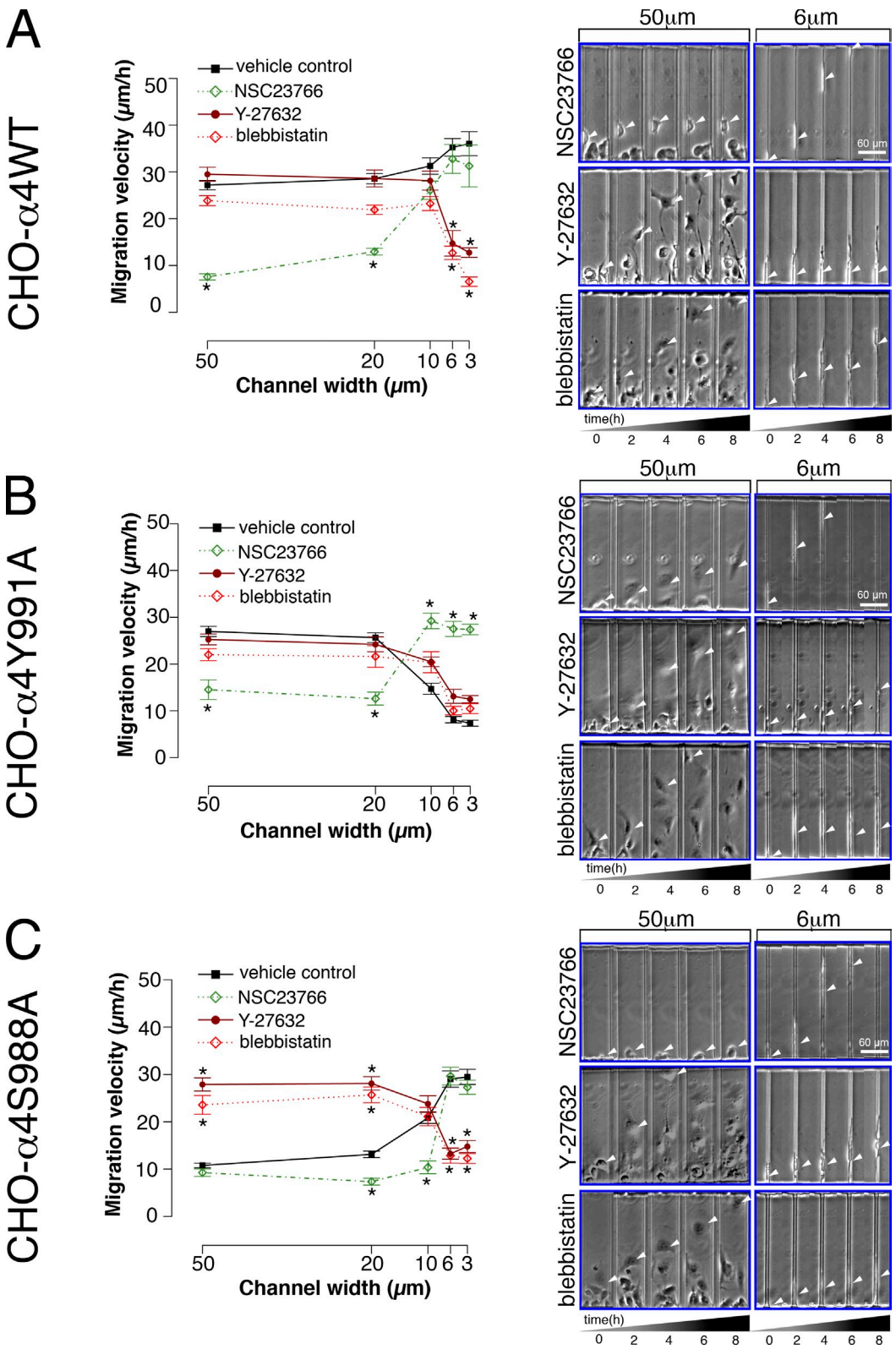

Figure 3. **Effects of inhibiting Rac1, ROCK, or myosin II on the migration of CHO-α4WT, CHO-α4Y991A, and CHO-α4S988A cells in microchannels.** (A–C) CHO-α4WT (A), CHO-α4Y991A (B), and CHO-α4S988A (C) cells were treated with either the Rac1 inhibitor NSC23766, the ROCK inhibitor Y-27632, the myosin II inhibitor blebbistatin, or vehicle control and allowed to migrate inside VCAM-1–coated channels. Their migration velocities in channels of different widths were quantified. Data represent means ± SEM of >40 cells from three independent experiments. *, $P < 0.005$ relative to control. The images of migrating cells in designated channel widths and time points are also shown. White arrowheads show the centroid of cell body.

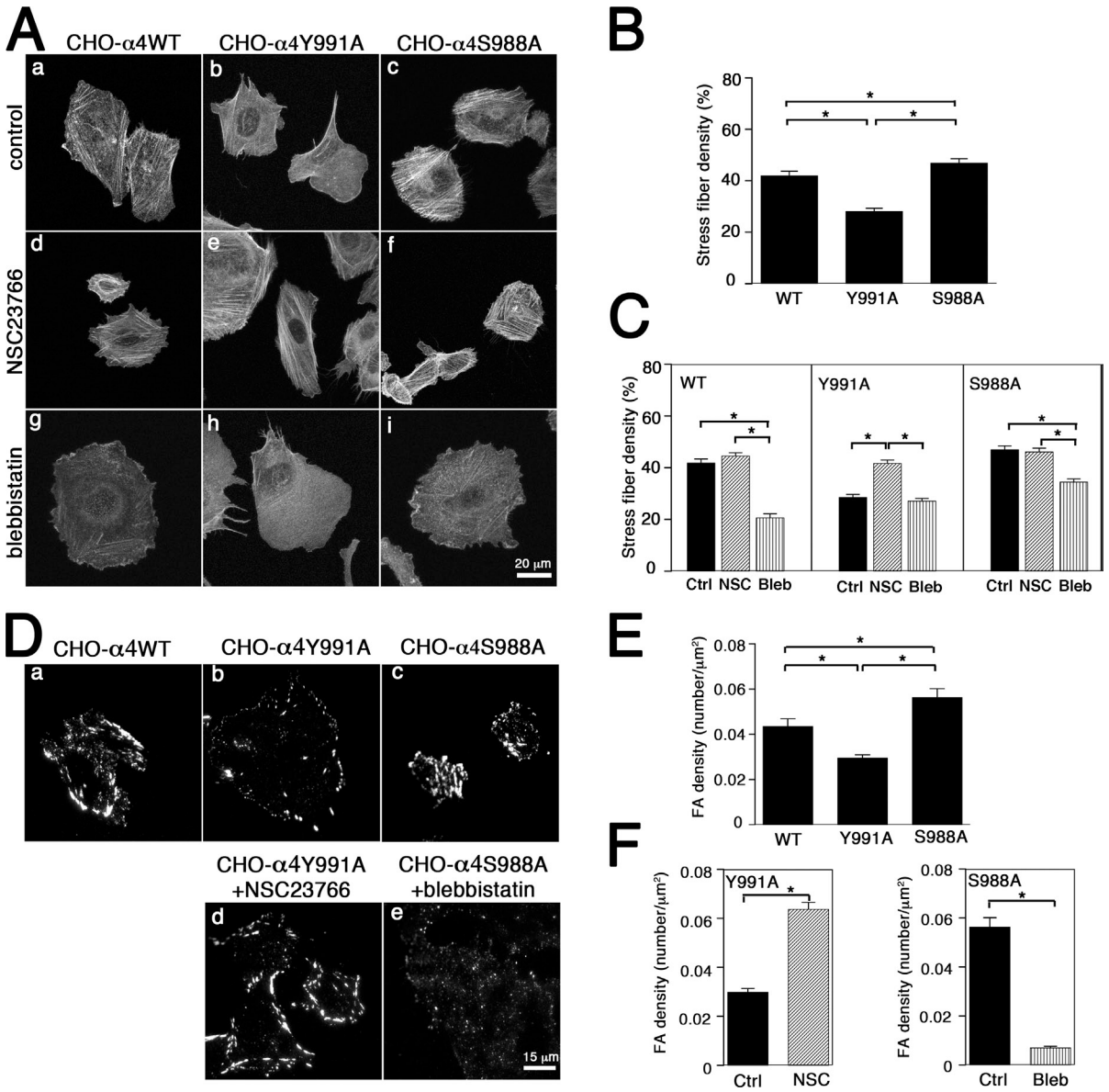

Figure 4. **Effects of inhibiting Rac1 or myosin II on stress fiber and focal adhesion densities in cells migrating on 2D surfaces.** CHO-α4WT, CHO-α4Y991A, or CHO-α4S988A cells were plated on VCAM-1–coated coverslips in the presence of vehicle control (A, a–c; and D, a–c), NSC23766 (A, d–f; and D, d), or blebbistatin (A, g–i; and D, e). (A) Cells were stained with TRITC-conjugated phalloidin and imaged by confocal microscopy. (B and C) Stress fiber density was measured and graphed as the percentage of total cell area occupied by stress fibers in wild experiments. *, $P < 0.05$ relative to control. (D) Cells were stained with an antibody against pY-paxillin and imaged by TIRF microscopy. (E and F) Focal adhesion density was measured as the number of focal adhesions (FA) per micrometer squared in the absence (E) or presence of NSC23766 for CHO-α4Y991A or blebbistatin for CHO-α4S988A cells (F). Data represent means ± SEM of 45 cells from three independent experiments. *, $P < 0.05$ relative to control. Ctrl, control.

in the microchannel assay. The efficacy of Rac1 depletion was verified by immunoblotting (Fig. S3 A). Our data reveal that Rac1 knockdown repressed cell migration in wide, but not narrow, channels (Fig. S3 A). Thus, inhibition of Rac1 activation in CHO-α4WT cells recapitulates the migratory phenotype of CHO-α4S988A cells in the microchannel assay. Because Rac1 can down-regulate myosin II via inhibition of RhoA-associated protein kinase (ROCK) or other mechanisms (Burridge and Wennerberg, 2004; Guilluy et al., 2011), we also tested the effects of the ROCK inhibitor Y-27632 (Liao et al., 2007) and myosin II ATPase cycle inhibitor blebbistatin (Limouze et al., 2004) on the migration velocity of CHO-α4WT cells. In 50-μm channels, CHO-α4WT cells treated with 45 μM Y-27632 or 50 μM blebbistatin displayed an abnormal migratory morphology similar to that reported by Even-Ram et al. (2007); the trailing edge failed to retract to the cell body and formed a long-tailed structure (Fig. 3 A and Video 2), whereas the leading edge exhibited increased lamellipodia protrusion. Neither Y-27632 nor blebbistatin significantly altered the migration velocity of CHO-α4WT cells in 50-, 20-, or 10-μm channels. In contrast, these agents effectively suppressed CHO-α4WT cell migration in narrow (6- and 3-μm) channels relative to controls (Fig. 3 A and Video 2). Notably, ROCK-1–depleted CHO-α4WT cells displayed a similar migratory phenotype to Y-27632– or

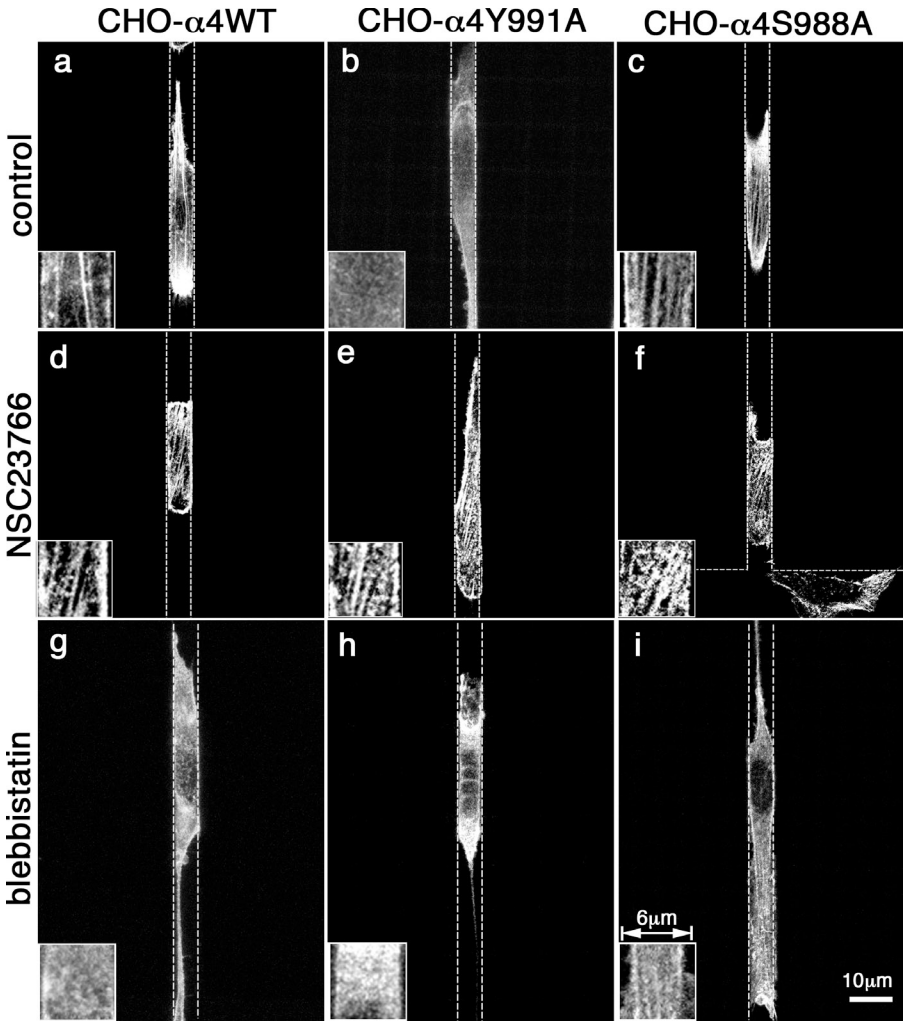

Figure 5. **Effects of inhibiting Rac1 or myosin II on stress fiber and focal adhesion densities in cells migrating inside 6-μm channels.** CHO-α4WT, CHO-α4Y991A, and CHO-α4Y988A cells were induced to migrate inside 6-μm VCAM-1–coated channels in the presence of vehicle control (a–c), NSC23766 (d–f), or blebbistatin (g–i). Cells were stained with TRITC-conjugated phalloidin and imaged by confocal microscopy. The boxes at the bottom left corner of each image show an enlarged view highlighting the stress fibers. The dotted lines indicate the PDMS walls of the channel.

blebbistatin-treated CHO-α4WT cells (Fig. S3 B). Thus, inhibition of the RhoA–myosin II pathway in CHO-α4WT cells recapitulates the migratory phenotype of CHO-α4Y991A cells in the microchannel assay.

These data show that the migration velocity of the α4β1 integrin–expressing CHO cells is modulated and optimized predominantly by Rac1 in wide channels, whereas the myosin II pathway attunes migration in narrow channels. Although the S988A mutation may suppress wide channel migration by inhibiting Rac1 activation (Goldfinger et al., 2003; Nishiya et al., 2005), we hypothesize that Y991A may repress narrow channel migration by enhancing Rac1 activity, which in turn negatively regulates myosin II contractility through a cross talk mechanism.

α4/paxillin binding regulates narrow channel migration through a cross talk between Rac1 and myosin II

To test this hypothesis, we first examined whether attenuation of Rac1 activity in CHO-α4Y991A cells alleviates the inhibitory effect of the Y991A mutation on α4β1-regulated narrow channel migration. Indeed, the treatment of CHO-α4Y991A cells with the Rac1 inhibitor NSC23766 greatly enhanced narrow channel migration (Fig. 3 B and Video 3). As expected, this intervention suppressed wide (50 and 20 μm) channel migration of CHO-α4Y991A cells (Fig. 3 B and Video 3). In line with previous observations showing that S988A mutation inhibits Rac1 activation (Goldfinger et al., 2003; Nishiya et al., 2005), NSC23766 treatment had little effect on the migration velocity of CHO-α4S988A cells through either wide (50 μm) or narrow (6 or 3 μm) channels compared with controls (Fig. 3 C). In contrast to NSC23766, Y-27632 and blebbistatin did not affect the migration of CHO-α4Y991A cells through wide or narrow channels (Fig. 3 B) but reversed the migratory phenotype of CHO-α4S988A cells, by markedly enhancing wide channel migration and suppressing narrow channel migration (Fig. 3 C). Therefore, suppression of narrow channel migration by Y991A mutation can be rescued by inhibiting Rac1, whereas suppression of wide channel migration by S988A can be rescued by inhibiting the myosin II pathway.

We next asked whether treatment with the Rac1 inhibitor NSC23766 enhanced myosin II activity in CHO-α4Y991A cells. Because the assembly of stress fibers depends on the contractile activities of myosin II, quantifying the formation of stress fibers is a valid measure of myosin II–driven contractility (Chrzanowska-Wodnicka and Burridge, 1996). Furthermore, tyrosine phosphorylation of paxillin (pY-paxillin) in focal adhesions depends on myosin II activity (Pasapera et al., 2010) and can also be used to evaluate cell contractile activity.

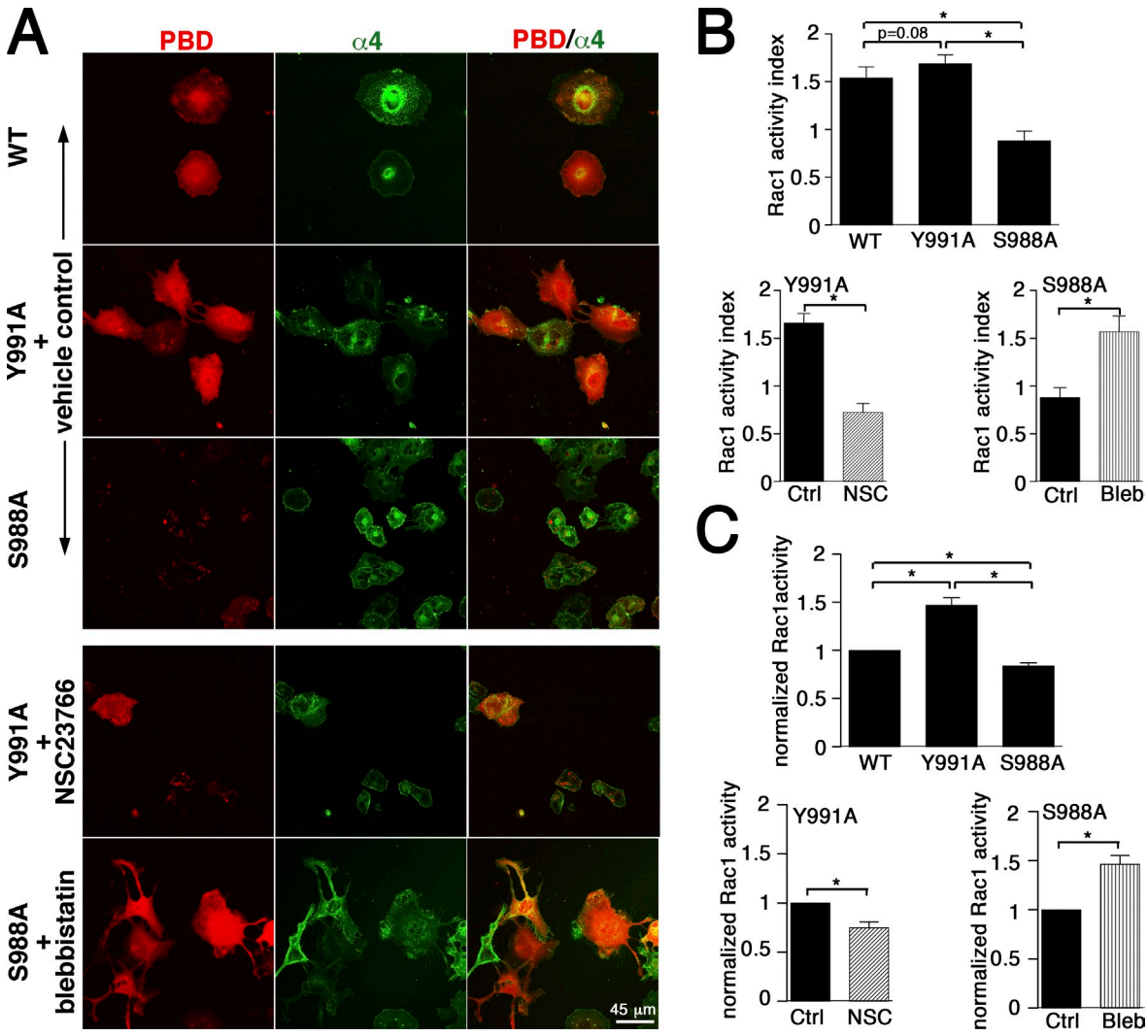

Figure 6. **Effects of Rac1 or myosin II inhibitors on Rac1 activity.** (A) CHO-α4WT, CHO-α4Y991A, and CHO-α4S988A cells transfected with RFP-PAK-PBD were plated on VCAM-1 and imaged for GTP-loaded Rac1 (red) and GFP-tagged α4 integrin by dual-color confocal microscopy in the presence of vehicle control, NSC23766 (NSC) for CHO-α4Y991A, or blebbistatin for CHO-α4S988A. (B) Rac1 activity was quantified by measuring the RFP-PAK-PBD red fluorescence intensity for each cell type normalized by GFP-tagged α4 integrin. Data represent means ± SEM of ≥50 cells from two independent experiments. (C) The overall level of GTP-loaded Rac1 was quantified in the presence of vehicle control or indicated treatments using ELISA. Data represent means ± SEM from four independent experiments. *, $P < 0.05$. Ctrl, control; Bleb, blebbistatin.

When plated on VCAM-1–coated glass coverslips, CHO-α4S988A cells had the highest densities of stress fibers (Fig. 4, A–C) and pY-paxillin–positive focal adhesions (Fig. 4, D–F), whereas CHO-α4Y991A cells had the lowest. Notably, the stress fiber and focal adhesion defects in CHO-α4Y991A cells were rescued when the cells were treated with the Rac1 inhibitor NSC23766 (Fig. 4, A [e], C, D [d], and F). On the other hand, the NSC23766 treatment did not have any significant effect on the stress fiber density of either CHO-α4WT or CHO-α4S988A cells. To confirm that the changes in stress fiber density reflect altered myosin II activity, we showed that blebbistatin significantly suppressed stress fiber density in CHO-α4WT and CHO-α4S988A cells (Fig. 4, A [g and i] and C). Moreover, blebbistatin also dramatically reduced the density of pY-paxillin–positive focal adhesion in CHO-α4S988A cells (Fig. 4, D [e] and F). However, blebbistatin failed to significantly suppress the already low stress fiber density of CHO-α4Y991A cells (Fig. 4 C). Similar stress fiber phenotypes were observed when the cells migrated inside 6-μm channels (Fig. 5). Under this confined condition, CHO-α4WT and CHO-α4S988A cells formed arrays of stress fibers that were aligned parallel to the channels (Fig. 5, a and c). In contrast, stress fibers were not detected in CHO-α4Y991A cells, but this stress fiber defect was rescued by treating cells with NSC23766 (Fig. 5, b and e). Blebbistatin treatment, as expected, diminished stress fibers (Fig. 5, g–i). Therefore, myosin II activity is reduced when α4/paxillin binding is disrupted by Y991A, and this can be rescued by Rac1 inhibition. We conclude that α4/paxillin binding promotes narrow channel migration by maintaining a high level of myosin II activity via its negative effect on Rac1.

We also quantified the activity of Rac1 in CHO-α4WT, CHO-α4Y991A, and CHO-α4S988A cells using a p21-activated kinase (PAK)–p21-binding domain (PBD) fluorescent probe (Fig. 6, A and B) or ELISA (Fig. 6 C). In both assays, Rac1

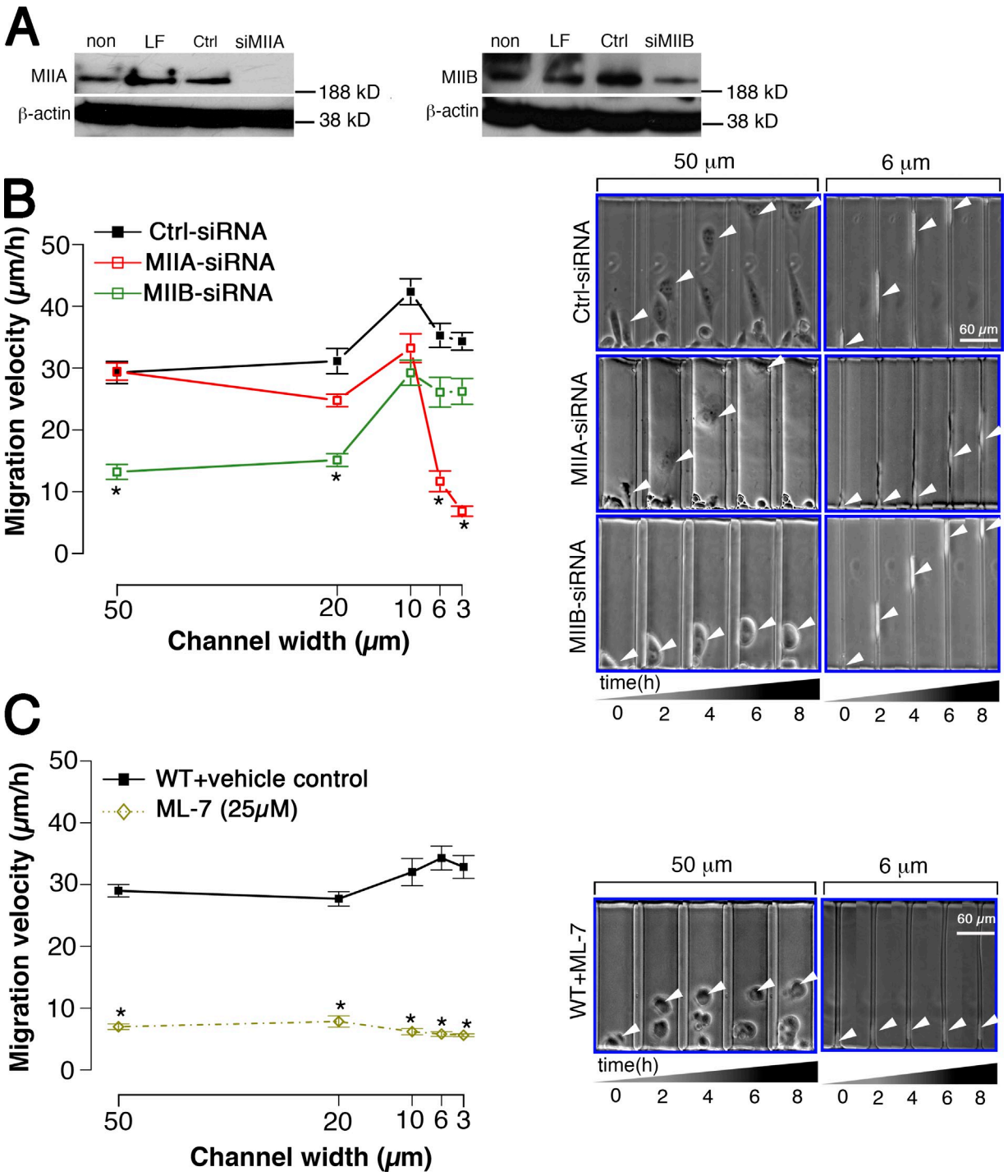

Figure 7. **Effects of MIIA or MIIB depletion on the migration of CHO-α4WT cells in microchannels.** (A) CHO-α4WT cells were either transfected with an siRNA for MIIA (a) or MIIB (b), a control (Ctrl) siRNA, with lipofectamine only (LF), or remained untransfected (non). The depletion of either MIIA or MIIB by their corresponding siRNAs was demonstrated by immunoblotting using an anti-MIIA or anti-MIIB antibody. β-Actin served as an internal control. (B) The migration velocities of MIIA- or MIIB-depleted CHO-α4WT cells and siRNA controls were quantified as a function of channel width. (C) The migration velocity of CHO-α4WT cells, treated with either ML-7 or a vehicle control, was measured in channels of different widths. In B and C, all channels were coated with VCAM-1. Data represent means ± SEM of >45 cells from three independent experiments. *, $P < 0.005$. The images of cells migrating inside 50- or 6-μm microchannels at designated time points are also shown. White arrowheads show the centroid of the cell body.

activity was the highest in CHO-α4Y991A cells, and it was inhibited by NSC23766. In contrast, Rac1 activity was the lowest in CHO-α4S988A cells. Notably, it was markedly increased by blebbistatin, thereby revealing that the inhibitory effect of the α4S988A mutation on Rac1 and the concomitant migration defect in wide channels can be rescued by a negative feedback of myosin II to Rac1.

Collectively, our data show that CHO-α4WT cells can migrate efficiently in both wide and narrow channels but through distinct mechanisms. In wide channels, a high level of Rac1 activity

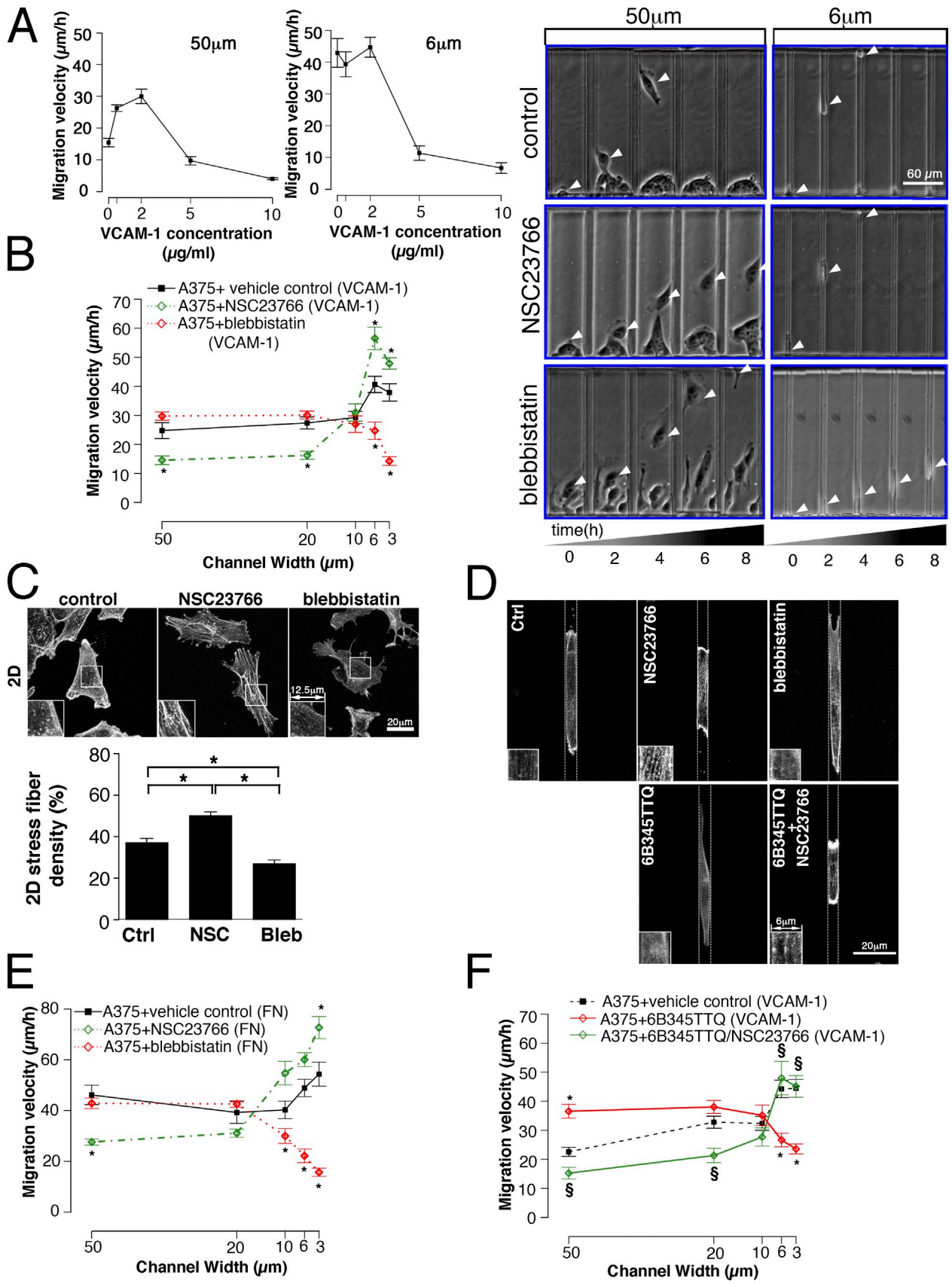

Figure 8. **Migration of A375-SM cells in microchannels.** (A–F) A375-SM cells were induced to migrate in microchannels coated with VCAM-1 (A–D) or fibronectin (E–F). (A) Migration velocity of A375-SM cells as a function of VCAM-1–coating concentration in 50- and 6-μm microchannels. (B and E) A375-SM cells were treated with NSC23766, blebbistatin, or vehicle control, and their migration velocities in channels of different widths were quantified. In B, the images of cells migrating inside the 50- or 6-μm channels at designated time points are shown. White arrowheads show the centroid of the cell body.

is maintained in cells when myosin II activity is low and the binding between α4 integrin and paxillin is suppressed by Ser^{988} phosphorylation at the α4 tail. This allows efficient cell migration in wide channels. In contrast, in narrow channels, myosin II activity is enhanced by α4/paxillin binding through Rac1 inhibition, which promotes efficient migration in narrow channels. Both wide and narrow channel migration involve Rac1–myosin II cross talk.

MIIA and MIIB have distinct roles in wide versus narrow channel migration

The differential effects of blebbistatin on wide versus narrow channel migration prompted us to examine the relative contributions of nonmuscle myosin II isoforms to cell migration through these microchannels. The major nonmuscle myosin II isoforms, IIA (MIIA) and IIB (MIIB), share the basic ATPase-dependent motor functions of binding and contracting F-actin, but they have distinct enzymatic kinetics (Kelley et al., 1996), subcellular distributions (Kelley et al., 1996; Cai et al., 2006), and functions (Stroka and Aranda-Espinoza, 2011). We knocked down each isoform in CHO-α4WT cells by transiently expressing MIIA or MIIB siRNA in the cells. The efficacy of MIIA or MIIB depletion was verified by immunoblotting (Fig. 7 A). MIIA-depleted CHO-α4WT cells exhibited increased lamellipodia protrusion and a trailing tail phenotype (Fig. 7 B and Video 4) similar to that displayed by MIIA-depleted fibroblasts (Even-Ram et al., 2007; Doyle et al., 2009) and blebbistatin- and Y-27632–treated CHO-α4WT cells (Fig. 3). Like the blebbistatin and Y-27632 treatments, MIIA depletion in CHO-α4WT cells failed to alter wide (50 and 20 µm) channel migration but markedly suppressed narrow (6 and 3 µm) channel migration (Figs. 7 B and S4 and Video 4). In distinct contrast, MIIB-depleted CHO-α4WT cells exhibited poor spreading (Figs. 7 B and S4 and Video 4), resulting in a dramatic reduction of wide channel migration (Fig. 7 B and Video 4), whereas the inhibitory effect became less pronounced as the channel width decreased ($P > 0.06$ at 6- and 3-µm channels). Furthermore, the inhibitory effects of MIIA or MIIB siRNA were rescued by cotransfection of siRNA-insensitive MIIA or MIIB, respectively (Fig. S4). Thus, although depleting MIIA had similar effects as blebbistatin and Y-23766, depleting MIIB displayed similar effects as the Rac1 inhibitor NSC27632.

Both MIIA and MIIB are activated by myosin light chain kinase (MLCK). We therefore tested the effect of blocking MLCK by treating cells with a specific MLCK inhibitor, ML-7 (25 µM). This intervention suppressed cell spreading and inhibited CHO-α4WT cell migration in both wide and narrow channels (Fig. 7 C and Video 4).

Collectively, our data reveal that MIIA and MIIB have distinct roles in wide versus narrow channel migration. MIIA is required for narrow channel migration, and MIIB is needed for wide channel migration, whereas MLCK is required for both wide and narrow channel migration.

α4β1-mediated signaling pathway is required for the migration of invasive melanoma cells

α4β1 integrin is up-regulated in human primary invasive melanoma cells (Mostafavi-Pour et al., 2003; Ryu et al., 2007) and plays important roles in melanoma extravasation (Matsuura et al., 1996). Therefore, we tested an invasive melanoma cell line, A375-SM, which expresses high levels of endogenous α4β1 integrin. Like CHO-α4WT, A375-SM cells displayed a fibroblast-like morphology on VCAM-1– or fibronectin-coated surfaces. Moreover, A375-SM cells exhibited a similar dependence of migration velocity on VCAM-1 concentration as the α4β1-expressing CHO cells in wide and narrow channels (Figs. 2 A and 8 A). In VCAM-1– or fibronectin-coated microchannels, NSC23766 treatment suppressed wide (50 and 20 µm) channel migration but enhanced narrow (6 and 3 µm) channel migration (Fig. 8, B and E). In contrast, blebbistatin inhibited narrow channel migration without altering the migration velocity through wide channels (Fig. 8, B and E). Of note, blebbistatin-treated A375-SM cells displayed lamellipodia protrusion and trailing tail defects similar to those observed in blebbistatin-treated CHO-α4WT cells. NSC23766 treatment increased the stress fiber density of cells plated on a 2D surface (Fig. 8 C) and resulted in thicker stress fibers in cells migrating through 6-µm channels (Fig. 8 D). As expected, blebbistatin diminished stress fiber formation (Fig. 8, C and D). Thus, high stress fiber levels correlate with high cell migration potential in narrow channels, which is consistent with the data on CHO-α4WT cells.

We next tested the pharmacological inhibitor 6B345TTQ, which specifically disrupts α4/paxillin binding (Kummer et al., 2010). Similar to CHO-α4Y991A cells, treatment of A375-SM cells with 6B345TTQ increased migration velocity in wide channels but suppressed it in narrow channels (Fig. 8 F). Notably, these effects were abolished when A375-SM cells were cotreated with 6B345TTQ and NSC23766 (Fig. 8 F). NSC23766 also reversed the 6B345TTQ-induced suppression of stress fiber formation (Fig. 8 D). These results demonstrate that the signaling pathway involving α4/paxillin binding and the cross talk between Rac1 and myosin II is required for efficient migration of A375-SM cells in narrow channels.

We also treated A375-SM cells with an anti–α4 integrin-blocking antibody. This treatment markedly reduced the migration velocity in both wide and narrow channels (Fig. 9 A). Blebbistatin and NSC23766 rescued the migratory defect induced by the anti–α4 integrin antibody in wide and narrow channels, respectively (Fig. 9 A). Furthermore, blebbistatin and

(C and D) A375-SM cells were plated on a 2D surface (C) or induced to migrate inside a 6-µm channel (D) in the presence of vehicle control (Ctrl), NSC23766 (NSC), or blebbistatin (Bleb), stained with TRITC-conjugated phalloidin, and imaged by confocal microscopy. The boxes at the bottom left corner of each image show enlarged images of stress fibers. In C, the density of stress fibers was measured and graphed as a percentage of total cell spreading area occupied by stress fibers. In D, the dotted lines indicate the PDMS walls of the channel. Each data (A–E) represent means ± SEM of >40 cells from three independent experiments. *, $P < 0.005$ (B and E) or $P < 0.05$ (C). (F) A375-SM cells were treated with the α4/paxillin-binding inhibitor, 6B345TTQ, in the presence of NSC23766 or vehicle control. Cell migration velocities in channels of different widths were quantified. Data represent means ± SEM of >30 cells from two independent experiments for each channel width. *, $P < 0.005$ relative to control. §, $P < 0.005$ relative to 6B345TTQ treatment alone. FN, fibronectin.

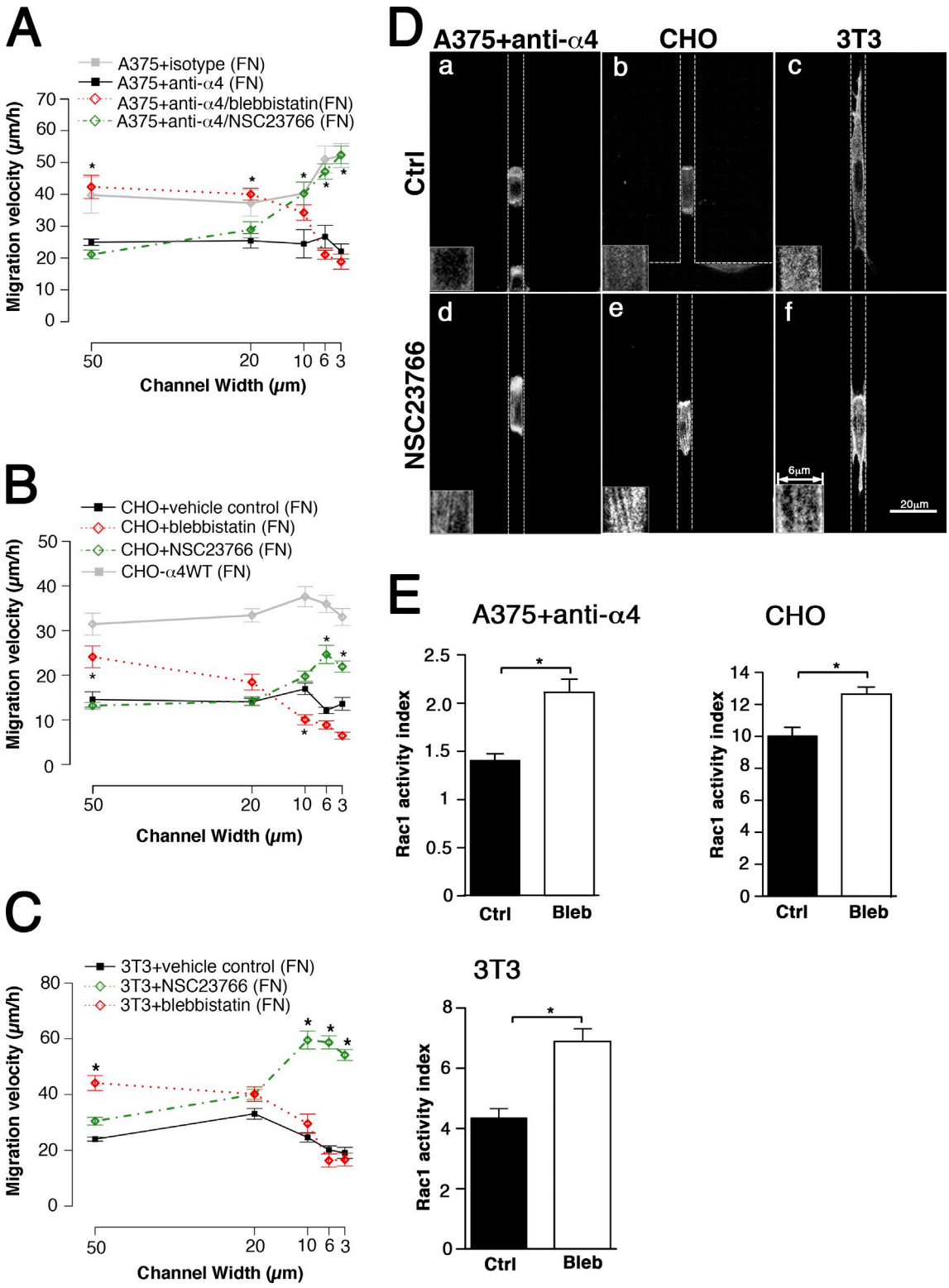

Figure 9. **Effects of Rac1 and myosin II inhibitors on the migration of anti-α4–treated A375-SM, CHO cells and 3T3 fibroblasts in microchannels.** (A–C) A375-SM cells treated with an anti–α4 integrin antibody or an isotype control (A), CHO cells (B), or 3T3 fibroblasts (C) were incubated with NSC23766, blebbistatin (Bleb), or the vehicle control (Ctrl) and allowed to migrate through microchannels coated with fibronectin (FN). Cell migration velocities in channels of different widths were quantified. CHO-α4WT cells treated with vehicle control were also included for comparison (B). Data represent means ± SEM of >30 cells from at least three independent experiments for each channel width. *, $P < 0.005$ relative to control. (D) Cells migrating inside 6-μm channels were stained with TRITC-conjugated phalloidin and imaged by confocal microscopy. The boxes at the bottom left corner of each image show enlarged images of stress fibers. The dotted lines indicate the PDMS walls of the channel. (E) Rac1 activity was quantified by measuring the RFP-PAK-PBD red fluorescence intensity for each cell type normalized by FITC intensity from background using dual-color broad-field microscopy. Data represent means ± SEM of ≥85 cells. *, $P < 0.05$.

NSC23766 increased the Rac1 activity and stress fibers, respectively, in anti–α4 integrin-treated A375-SM cells (Fig. 9, D and E). These results disclose the importance of α4β1 integrin in promoting the migration of A375-SM cells in both unconfined and confined spaces. Like CHO-α4WT cells, A375-SM cells optimize their motile activities by routing the α4β1-mediated signaling network to distinct targets in response to different physical microenvironments.

The migration of CHO cell and 3T3 fibroblast in wide and narrow channels is attenuated by myosin II and Rac1, respectively

The results from the anti–α4 integrin antibody experiments (Fig. 9, A, D, and E) suggest that the rescue by NSC23766 and blebbistatin in the microchannels could be a general phenomenon for fibroblast-like cells that are devoid of α4β1 integrin. To test this, we assessed the migratory potential of parental CHO cells and 3T3 fibroblasts in the microchannel assay in the presence and absence of NSC23766 or blebbistatin. In line with anti–α4 integrin-treated A375-SM cells, the parental CHO cells displayed a reduced migration velocity compared with CHO-α4WT cells in fibronectin-coated wide and narrow channels; blebbistatin and NSC23766 increased CHO cell migration velocity in wide and narrow channels, respectively (Fig. 9 B). Moreover, blebbistatin and NSC23766 increased Rac1 activity and stress fiber density of CHO cells, respectively (Fig. 9, D and E). Similar observations were made with 3T3 fibroblasts (Fig. 9, C–E). These data demonstrate that, in fibroblasts, myosin II and Rac1 can function as breaks through a cross talk mechanism to attenuate the migration of the cells on unconfined and confined microenvironments, respectively.

The migration of T lymphocyte is promoted by α4/paxillin binding and the downstream Rac1–myosin II cross talk pathway

α4β1 integrin is highly expressed in T lymphocytes (Yednock et al., 1992). T lymphocytes display an ameboidal mode of migration, which is distinct from that of fibroblast-like cells such as α4β1 integrin–expressing CHO and A375-SM melanoma cells. We thus sought to investigate the migratory phenotype of the Jurkat T cell line and primary T cells. Reminiscent to CHO-α4WT and A375-SM cells migrating in narrow channels, the migration velocity of Jurkat T cells was suppressed by blebbistatin but was enhanced by NSC23766, albeit in all channels (Fig. 10 A). The migratory potential of T cells on 2D is negatively correlated with their spreading area (Jacobelli et al., 2010). Thus, we also measured this parameter. Blebbistatin and NSC23766 increased and reduced, respectively, the spreading area of Jurkat T cells on VCAM-1–coated 2D surfaces (Fig. 10 D). To determine whether α4/paxillin binding contributes to Jurkat T cell migration, cells were treated with 22.5 μM 6B345TTQ, which specifically disrupts α4/paxillin binding. 6B345TTQ significantly reduced the migration of Jurkat T cells in all channels and increased their spreading area (Fig. 10, B and E), which is in line with published data on 2D (Kummer et al., 2010). Furthermore, cotreatment with 6B345TTQ and NSC23766 abolished the effect of 6B345TTQ on the migration velocity and cell spreading (Fig. 10, B and E).

We also tested primary $CD4^+$ T cells isolated from mice carrying the α4Y991A mutation generated by gene targeting (referred as to α4Y991A-$CD4^+$; Féral et al., 2006) and those from WT mice (referred as to WT-$CD4^+$). α4Y991A-$CD4^+$ cells exhibited larger spreading area when plated on 2D surface and reduced migration velocities relative to WT-$CD4^+$ in all channels (Fig. 10, C and F), which is in concert with the reported spreading and migration phenotypes of Jurkat T cells carrying the α4Y991A mutation (Liu et al., 1999). Notably, the migration and spreading defects of α4Y991A-$CD4^+$ cells were rescued by NSC23766 (Fig. 10, C and F). We thus conclude that α4/paxillin binding and its inhibitory effect on Rac1 promotes effective migration of T cells via Rac1–myosin II cross talk, which is analogous to the migration of CHO-α4WT and A375-SM cells in narrow channels.

Discussion

Our microchannel assay provides a systematic means to examine migratory behaviors in response to varying degrees of confinement, in which the absence of confinement (wide channels in which $W > d_{cell}$) mimics a 2D environment. This enables us to directly compare and contrast 2D versus confined migration in a quantitative manner and to elucidate the mechanisms underlying these two regimes. Using this assay, we examined several fibroblast-like cell types expressing or lacking α4β1 integrin. Fibroblast-like cells, including the α4β1 integrin–expressing CHO cells and A375-SM cells, use a mesenchymal mode of migration on 2D surfaces, in which lamellipodia protrusion and cell–ECM adhesion play critical roles. In contrast, cells migrating through physically confined spaces display less extensive protrusive activity at the leading edge. This migration mode depends on myosin II–driven contractility, akin to ameboid migration of T lymphocytes (Yoshida and Soldati, 2006; Jacobelli et al., 2010). Unlike lymphocytes, however, CHO-α4WT and A375-SM cells in narrow channels retain well-organized stress fibers, which are reminiscent of those observed in fibroblasts in a 3D linear elastic environment or under other forms of physical constraints (Doyle et al., 2009; Ghibaudo et al., 2009; Petrie et al., 2012). It is possible that in response to the physical constraints, fibroblast-like cells switch their migration mode to become more ameboid-like while still retaining some mesenchymal characteristics; specific cell types may possess certain degrees of mesenchymal or ameboid characteristics. In response to confinement or other physical constraints, the cells may undergo different degrees of mesenchymal-to-ameboid transition, during which the strategy for optimizing cell migration has to be altered. It can be envisioned that myosin II–driven contractility of fibroblast-like cells may facilitate confined migration by laterally constraining the cell body, thus minimizing cell substrate contact interactions (Sixt, 2012). On the other hand, Rac1-dependent lamellipodia protrusion rather than the myosin II–driven contractility becomes more critical in 2D migration. To adapt to different degrees of confinement, the cells optimize the signaling network by adjusting the balance between Rac1 and myosin II activities.

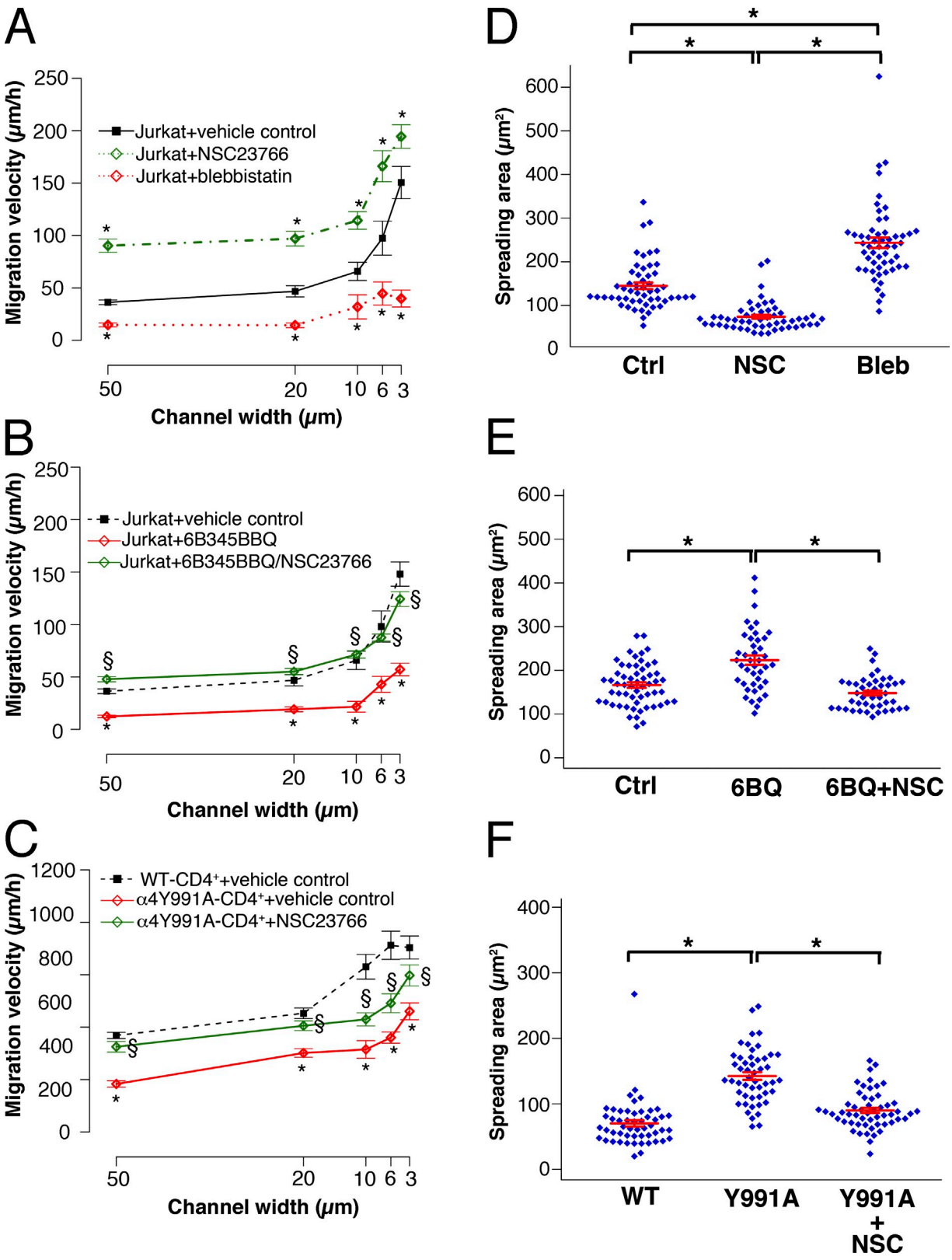

Figure 10. **Effects of Rac 1 and myosin II inhibitors on the migration of Jurkat T and primary CD4⁺ T cells in microchannels.** (A and D) Jurkat T cells were treated with NSC23766 (NSC), blebbistatin (Bleb), or vehicle control (Ctrl). (B and E) Jurkat T cells were treated with the α4/paxillin-binding inhibitor, 6B345TTQ, or vehicle control or treated with 6B345TTQ (6BQ) plus NSC23766 or vehicle control. (C and F) Primary WT-CD4⁺ or Y991A-CD4⁺ T cells were treated with vehicle control or NSC23766. Cells were either induced to migrate through channels of different widths (A–C) or plated on a 2D surface (D and E). All surfaces were coated with VCAM-1. Cell migration velocities (A–C) and mean spreading areas (D and E) were quantified. Data represent means ± SEM of >60 cells. *, $P < 0.005$ relative to control (A and B) or WT-CD4⁺ T cells (C). §, $P < 0.005$ compared with the absence of NSC23766.

The α4/paxillin-mediated signaling network (Fig. S5) provides a paradigm for such adaptation in response to altered physical environment. On a 2D surface, α4β1 integrin promotes the migration of CHO-α4WT cells by optimizing Rac1 activity at the cell front (Goldfinger et al., 2003). The elevated Rac1 activity is maintained by Ser^{988} phosphorylation at the α4 tail that prevents α4/paxillin binding. In contrast, as cells experience increasing degrees of confinement, α4/paxillin binding becomes progressively indispensable for effective migration. Therefore, the levels of α4/paxillin binding and Ser^{988} phosphorylation are modulated as CHO-α4WT cells migrate in different microenvironments. The mechanism of this signaling adaptation in response to physical confinement is beyond the scope of this paper, but we can envision three possible mechanisms. First, Ser^{988} phosphorylation and its downstream targets could be regulated via α4β1-ligand engagement, in which α4β1 integrin functions as a mechanosensor. For instance, it has been reported that engagement of α4β1-specific ligand down-regulates RhoA and stress fiber formation in A375 cells plated on 2D surfaces (Moyano et al., 2003). Although our data show that under confinement VCAM-1 is not required for CHO-α4WT and A375-SM cells to reach maximum migration velocities, ECM proteins, such as fibronectin, may be secreted by the cells over the course of the microchannel assay and/or deposited from the chemoattractant (FBS) source, thereby providing force signals. This opens a second possibility: other integrins or cell surface receptors may act as mechanosensors (Jalali et al., 2001; Li et al., 2002; Roca-Cusachs et al., 2012) that regulate the cellular responses to physical confinement. A third possible mechanism is that the cytoskeleton itself may function as a mechanosensor (Janmey and Weitz, 2004; Ren et al., 2009; Schwarz and Gardel, 2012). The actomyosin network may sense the mechanical cues generated by confinement-induced cell shape changes (McBeath et al., 2004), leading to the observed cellular responses.

We show that disrupting α4/paxillin binding in α4β1-expressing CHO and A375-SM cells inhibits myosin II–driven contractility, and this defect can be rescued by treating cells with a Rac1 inhibitor. Likewise, treatment of fibroblasts and CHO cells lacking α4β1 integrin with the Rac1 inhibitor augments migration in narrow channels by promoting myosin II–driven contractility. Moreover, blebbistatin increases migration velocity in wide channels via enhancement of Rac1 activity. We further show that the Rac1 inhibitor also has a rescue effect on primary $CD4^+$ T cells carrying the α4Y991A mutation, which is similar to that of CHO-α4WT and A375-SM cells under confinement. These observations support a cross talk mechanism in which Rac1 and myosin II negatively regulate each other to modulate cell motility (Fig. S5). Cross talk between Rac1 and myosin II and vice versa has been reported by numerous studies (Burridge and Wennerberg, 2004; Bustos et al., 2008). Rac1 can inhibit myosin II–driven contractility by several mechanisms. For example, Rac1 can inhibit Rho by activating p190RhoGAP (Nimnual et al., 2003). Rac1 can also inhibit myosin II activities by promoting phosphorylation of MLCK (Sanders et al., 1999) or myosin II heavy chain (Leeuwen et al., 1997) via PAK or by inhibiting phosphorylation of myosin II regulatory light chain via WAVE2 (Sanz-Moreno et al., 2008).

Our data reveal that MIIB but not MIIA is required for optimizing 2D migration, whereas this scenario is reversed for confined migration. These observations are in agreement with published data showing that MIIB and MIIA have overlapping but differential functions in cell migration. MIIA is required for stress fiber formation, cellular contractility, and trailing edge retraction (Even-Ram et al., 2007; Vicente-Manzanares et al., 2007, 2011). It has been proposed that MIIA is the predominant downstream target for the Rho pathway, which is based on observations showing that MIIA depletion has similar effects as blebbistatin or Y-27632 treatment (Sandquist et al., 2006). Indeed, we also observed that MIIA depletion had similar effects as inhibiting ROCK or the enzyme cycle of myosin II; all interventions impaired confined, but not 2D, migration, thus suggesting that MIIA-driven contractility is critical for the efficient migration of CHO-α4WT cells under physical confinement (Fig. S5). In contrast to MIIA, MIIB plays a relatively minor role in cellular contractility, as demonstrated by traction force measurements and stress fiber evaluations of MIIA- and MIIB-deficient mouse embryonic fibroblasts (Cai et al., 2006). Instead, MIIB stabilizes front–back polarity of migrating cells (Vicente-Manzanares et al., 2007, 2011) and contributes to leading edge protrusion (Giannone et al., 2007). Consistent with these studies, we have shown that MIIB-depleted CHO-α4WT cells on 2D substrates exhibited a rounded morphology and polarity defects, which greatly inhibited 2D migration. However, this molecular intervention had little or no inhibitory effect on confined migration. Inhibition of MLCK impairs the activation of both MIIA and MIIB, leading to reduced migration in both wide and narrow channels. This observation suggests that in wide channels MIIB depletion may be dominant over the potential elevation of Rac1 induced by suppressed MIIA activity.

Altogether, our study reveals that distinct mechanisms regulate cell migration in 2D versus confined spaces, which involves Rac1–myosin II cross talk. The α4β1-mediated pathway provides a paradigm for the plasticity of cells in which a signaling network can be tuned in distinct manners in response to different physical conditions to achieve maximal cell motility. Future work should be directed toward elucidating how the mechanical signals generated by physical confinement induce cellular responses and how cells alter their signaling strategies to optimize cell motility. It is also important to determine how spatial alterations of the signaling molecules result in localized activity for efficient cell migration in confinement.

Materials and methods

Cell culture, pharmacological inhibitors, plasmids, and transfection

CHO-α4WT, CHO-α4Y991A, or CHO-α4S988A cell lines were generated by stably transfecting CHO cells with pQN4G, pQN4Y991AG, or pQN4S988AG plasmids, in which WT or mutant α4 integrin cDNA was inserted into a PGBI25-fN1 GFP vector (Pinco et al., 2002; Dikeman et al., 2008). The cells were maintained in Ham's F12 (10–080-CM; Cellgro; Corning) medium. CHO cells, 3T3 fibroblasts, and A375-SM cells were maintained in DMEM (high glucose; Life Technologies). Media were supplemented with 10% FBS (Gibco) and 1 µg/ml penicillin/streptomycin. For inhibitor experiments using fibroblast-like cells, 100 µM NSC23766 (EMD Millipore), 25 µM ML-7 (Sigma-Aldrich), 45 µM Y-27632 (Sigma-Aldrich), 50 µM blebbistatin (Cayman), 22.5 µM 6B345BBQ (Sigma-Aldrich), or appropriate vehicle controls were added to the cells seeded in serum-free

medium near microchannel entrances. Jurkat T cells and primary CD4+ cells were treated with 20 µM NSC23766, 75 µM blebbistatin, 90 µM 6B345TTQ, or appropriate vehicle controls. For antibody-blocking experiments, cells were treated with 3 µg/ml anti–α4 integrin mAb (clone P1H4; EMD Millipore). After 1 h of incubation with the inhibitors or antibody at 37°C, the chemoattractant (10% FBS) was added to topmost inlet port (Fig. 1) to induce cell migration. Rac1 siRNA, ROCK siRNA, and control siRNA were obtained from Santa Cruz Biotechnology, Inc. The pSUPER-MIIA, pSUPER-MIIB, and siRNA-insensitive MIIA and MIIB were gifts from A.F. Horwitz (University of Virginia, Charlottesville, VA). In pSUPER-MIIA and pSUPER-MIIB, the oligonucleotides 5′-GATCTGAACTCCTTCGAGC-3′ (IIA) and 5′-GGATCGCTACTATTCAGGA3′ (IIB) were inserted into the appropriate pSUPER cassette. In siRNA-insensitive MIIA and MIIB plasmids, MIIA and MIIB cDNA, each carrying a silent mutation, were inserted into an mCherry vector modified from pEGFP-C1 (Vicente-Manzanares et al., 2007). The RFP-PAK-PDB (in a modified pFUW vector) was a gift from P. Devreotes (Johns Hopkins University, Baltimore, MD). Transient transfection was performed using Lipofectamine 2000 (Life Technologies) according to the manufacturer's protocol. Knockdown efficiency was verified by Western blotting analysis using antibodies against MIIA (Sigma-Aldrich), MIIB (Santa Cruz Biotechnology, Inc.), and β-actin (Sigma-Aldrich).

Microfluidic-based microchannel assay

PDMS microchannels were fabricated using standard replica molding. Masks to generate the microchannel design were drawn using Illustrator CS2 (Adobe) and printed onto a transparency by a 5,080-dpi printer (PageWorks) or transferred to a chrome-on-glass photolithography mask (Advance Reproductions Corp.). To prepare masters, SU-8 2010 and SU-8 2025 epoxy-negative photoresists (Microchem Corp.) were applied by spin coating (Laurell Technologies Corp.) onto silicon wafers (Montco Silicon Technologies, Inc.) in two steps. SU-8 2010 was first spread at 600 rpm for 20 s and then at 4,000 rpm for 60 s to a final thickness of 8–10 µm. The photoresist was prebaked at 60°C for 1 min, exposed to UV (350−450 nm) radiation through appropriate masks for 40 s, postbaked at 115°C for 8 min, and subsequently developed using SU-8 developer. This step was used for generating the microchannels present in the final device. The second feature of the microfluidic-based microchannel master consisted of the cell seeding line and the FBS gradient generation line and was fabricated using the following steps: SU-8 2025 was first spread at 500 rpm for 10 s and then at 4,000 rpm for 30 s to a final thickness of 50 µm. The photoresist was prebaked at 80°C for 3 min and at 110°C for 6 min, cooled, and exposed to UV (350−450 nm) radiation for 30 s through a mask aligned with the previously fabricated microchannels. The photoresist was then exposed for 8 min at 110°C and developed as described in this paragraph. PDMS stamps were obtained by mixing prepolymer (Sylgard 184) with cross-linker (Dow Corning) in a 10:1 ratio (by weight), degassing in a vacuum, and curing at 80°C for 1 h. Each PDMS well inlet and outlet was punched out with a diameter of 6 mm. Both the PDMS device and microscope slide (Fisherfinest; Thermo Fisher Scientific) were cleaned and made hydrophilic using a plasma cleaner for 2 min. The PDMS device was then attached to a glass slide followed by precoating various concentrations of VCAM-1 at 37°C for 1 h. The microchannel was washed with PBS containing calcium/magnesium for 1 min before seeding cells. A total of 10^5 cells in a 50-µl volume was added to the cell inlet port. Chemotactic-driven cell migration was recorded via time-lapse microscopy (inverted Eclipse Ti microscope; Nikon) using software-controlled stage automation (Nikon). To calculate migration velocity, the cell center was identified as the midpoint between poles of the cell body and was tracked for changes in x, y position at 20-min intervals or 5-min intervals only for CD4+ T cells over a 10-h period.

Stress fiber imaging and quantification

Cells were either plated on coverslips overnight or induced to migrate through channels of prescribed widths coated with 1 µg/ml VCAM-1. The cells were then fixed with 3.7% formaldehyde for 10 min followed by permeabilization with 0.1% Triton X-100 for 10 min and a 30-min blocking at RT with 1% BSA. After washing 3× with PBS, cells were incubated with Alexa Fluor 568–conjugated phalloidin (1:500; Molecular Probes) for 1 h at RT. Images were captured at 12-bit depth on a microscope (Axiovert 200 Light Manager; Carl Zeiss) equipped with an laser confocal scanner (LSM 510 META; Carl Zeiss) and a 63×/1.4 NA oil immersion objective. For all acquisitions, detector voltage, scan speed, pixel resolution, laser power, and optical zoom were standardized and used consistently to ensure quantitative image analysis. Captured images were exported as raw uncompressed TIFF images. Images of phalloidin-stained cells were processed using the following steps to extract the values of stress fiber density in ImageJ (National Institutes of Health): (a) enhance intensity using default setting, (b) subtract the background, and (c) convert the processed image to black and white using the binary setting in ImageJ. Stress fiber area was identified as the pixels with a value of 255, distinguished from others pixels with a value of 0. Lastly, (d) stress fiber density was calculated as the percentage of total cell spreading area occupied by stress fiber area. To obtain 3D images of actin in various degrees of confinement, the 3D viewer in ImageJ was used to reconstruct serial z planes into a 3D rendering.

Focal adhesion imaging and quantification

Cells were plated on VCAM-1–coated coverslips and allowed to spread for ∼16 h and then fixed in 3.7% formaldehyde for 10 min, permeabilized in 0.5% Triton X-100 for 5 min, and blocked in 2.5% BSA for 1 h. Cells were immunostained using an antibody against pY-paxillin (Cell Signaling Technology) at 1:100 dilution for 2 h followed by an Alexa Fluor 568 secondary antibody (Invitrogen) at 1:100 dilution for 1 h. Cells were washed three times with PBS in between each step, and all steps were completed at RT. The stained cells were imaged by total internal reflection fluorescence (TIRF) microscopy using an inverted microscope (3i Marianas; Intelligent Imaging Innovations, Inc.) equipped with dual electron multiplying charge-coupled device cameras (Cascade II:512; Photometrics) for simultaneous two-channel TIRF acquisition, along with a 100×/NA 1.45 oil immersion lens and SlideBook 8.0 software (Intelligent Imaging Innovations, Inc.). TIRF images were processed and quantified as previously described (Stroka and Aranda-Espinoza, 2011; Stroka et al., 2012). In brief, images were made binary, and the particle analyzer tool was used in ImageJ to measure pY-paxillin–positive punctate areas >0.1 μm^2, total focal adhesion area, or number of focal adhesions per area. Total cell area for each image was determined by tracing α4-GFP–positive areas on TIRF images. TIRF experiments were repeated three times, for a total of 40–60 cells per condition.

T cell isolation

Mice were kept in accordance with guidelines of the Johns Hopkins University Institutional Animal Care and Use Committee. α4Y991A mice carrying a targeted α4Y991A mutation, backcrossed into a C57BL/6 background, were a gift from M.H. Ginsberg (University of California, San Diego, La Jolla, CA; Féral et al., 2006). WT C57BL/6 mice were obtained from Jackson ImmunoResearch Laboratories, Inc. The mice were sacrificed via CO_2 asphyxiation. Spleens and lymph nodes were collected and homogenized, and red blood cells were lysed. CD4+ T cells were purified using magnetically labeled beads (Miltenyi Biotec) according to the manufacturer's protocol. Cells were then cultured in 50% RPMI 1640/50% Eagle's Ham's amino acids media supplemented with 10% heat-inactivated low-lipopolysaccharide FBS, 1% penicillin/streptomycin, and 1% glutamine and stimulated with plate-bound anti-CD3 (145-2C11) in combination with 2 µg/ml anti-CD28 antibodies for 72 h.

Rac1 activity measurement by ELISA

The Rac1 activity was measured using the G-LISA Rac Activation Assay kit (Cytoskeleton, Inc.). In brief, CHO-α4WT, CHO-α4Y991A, or CHO-α4S988A cells were plated on 1 µg/ml VCAM-1 for 12 h in the presence of select inhibitors or appropriate vehicle control. Cell lysates were then prepared and incubated on Rac-GTP affinity plates followed by incubation with an anti-Rac1 antibody. The signal was determined by measuring absorbance at 600 nm using a microplate reader.

Rac 1 activity measurement using a Rac1 probe

Cells were transfected with 1 ng/ml RFP-PAK-PDB. After 48 h of transfection, the cells were treated with the designated inhibitors or appropriated vehicle controls. Live images were taken by either broad field (inverted Eclipse Ti microscope) or confocal (Axiovert 200 Light Manager as described in Stress fiber imaging and quantification) dual-color fluorescent microscopy. The activated Rac1 level was quantified by averaging TRITC intensity normalized by averaged FITC intensity of the cells. For the α4 integrin–expressing CHO cells, the FITC intensity was extracted from expression of GFP-tagged α4 integrin. For A375, 3T3, and CHO cells, FITC intensity was extracted from background.

Statistical analysis

Data are expressed as means ± SEM. Statistical significance of differences between means was determined by Student's *t* test or one-way analysis of variance followed by the Tukey test for multiple comparisons, where appropriate.

Online supplemental material

Fig. S1 shows the surface expression levels of α4 integrin in CHO-α4WT, CHO-α4Y991A, and CHO-α4S988A cells. Fig. S2 presents the quantitative analysis of velocity, speed, and chemotactic index of α4 integrin–expressing CHO, A375-SM, and Jurkat T cells in wide and narrow channels. Fig. S3 validates the effects of Rac1 and ROCK-1 depletion on the migration of CHO-α4WT cells via RNAi. Fig. S4 shows the rescue of migration defect of MIIA or MIIB depletion by cotransfection with mCherry-MIIA or mCherry-MIIB in CHO-α4WT cells. Fig. S5 presents the model and summary of α4 tail–mediated signaling in optimizing 2D and confined migration. Video 1 shows migration of CHO-α4WT, CHO-α4Y991A, and CHO-α4S988A cells through 50- and 6-µm channels. Video 2 shows migration of NSC23766-, Y-27632–, or blebbistatin-treated CHO-α4WT cells through 50- and 6-µm channels. Video 3 shows migration of NSC23766-, Y-27632–, or blebbistatin-treated CHO-α4Y991A cells through 50- and 6-µm channels. Video 4 shows migration of MIIA-depleted, MIIB-depleted, or ML-7–treated CHO-α4WT through 50- and 6-µm channels. Online supplemental material is available at http://www.jcb.org/cgi/content/full/jcb.201302132/DC1.

We thank Mark Ginsberg for providing α4Y991A mice and Peter Devreotes and Alan F. Horwitz for providing plasmids. We also thank Susan Craig for her critical reading and Nicholas Barbera for technical assistance.

This work was supported by grants from the National Cancer Institute (U54-CA143868, CA101135, and F32-CA177756), National Institutes of Health (GM63710), National Science Foundation (NSF-1159823), and Kleberg Foundation.

Submitted: 25 February 2013
Accepted: 26 July 2013

References

Alexander, S., G.E. Koehl, M. Hirschberg, E.K. Geissler, and P. Friedl. 2008. Dynamic imaging of cancer growth and invasion: a modified skin-fold chamber model. *Histochem. Cell Biol.* 130:1147–1154. http://dx.doi.org/10.1007/s00418-008-0529-1

Balzer, E.M., Z. Tong, C.D. Paul, W.C. Hung, K.M. Stroka, A.E. Boggs, S.S. Martin, and K. Konstantopoulos. 2012. Physical confinement alters tumor cell adhesion and migration phenotypes. *FASEB J.* 26:4045–4056. http://dx.doi.org/10.1096/fj.12-211441

Berlin, C., R.F. Bargatze, J.J. Campbell, U.H. von Andrian, M.C. Szabo, S.R. Hasslen, R.D. Nelson, E.L. Berg, S.L. Erlandsen, and E.C. Butcher. 1995. alpha 4 integrins mediate lymphocyte attachment and rolling under physiologic flow. *Cell*. 80:413–422. http://dx.doi.org/10.1016/0092-8674(95)90491-3

Burridge, K., and K. Wennerberg. 2004. Rho and Rac take center stage. *Cell*. 116:167–179. http://dx.doi.org/10.1016/S0092-8674(04)00003-0

Bustos, R.I., M.A. Forget, J.E. Settleman, and S.H. Hansen. 2008. Coordination of Rho and Rac GTPase function via p190B RhoGAP. *Curr. Biol.* 18:1606–1611. http://dx.doi.org/10.1016/j.cub.2008.09.019

Cai, Y., N. Biais, G. Giannone, M. Tanase, G. Jiang, J.M. Hofman, C.H. Wiggins, P. Silberzan, A. Buguin, B. Ladoux, and M.P. Sheetz. 2006. Nonmuscle myosin IIA-dependent force inhibits cell spreading and drives F-actin flow. *Biophys. J.* 91:3907–3920. http://dx.doi.org/10.1529/biophysj.106.084806

Chen, S.H., W.C. Hung, P. Wang, C. Paul, and K. Konstantopoulos. 2013. Mesothelin binding to CA125/MUC16 promotes pancreatic cancer cell motility and invasion via MMP-7 activation. *Sci Rep*. 3:1870.

Chrzanowska-Wodnicka, M., and K. Burridge. 1996. Rho-stimulated contractility drives the formation of stress fibers and focal adhesions. *J. Cell Biol.* 133:1403–1415. http://dx.doi.org/10.1083/jcb.133.6.1403

Dikeman, D.A., L.A. Rivera Rosado, T.A. Horn, C.S. Alves, K. Konstantopoulos, and J.T. Yang. 2008. alpha4 beta1-Integrin regulates directionally persistent cell migration in response to shear flow stimulation. *Am. J. Physiol. Cell Physiol.* 295:C151–C159. http://dx.doi.org/10.1152/ajpcell.00169.2008

DiMilla, P.A., J.A. Stone, J.A. Quinn, S.M. Albelda, and D.A. Lauffenburger. 1993. Maximal migration of human smooth muscle cells on fibronectin and type IV collagen occurs at an intermediate attachment strength. *J. Cell Biol.* 122:729–737. http://dx.doi.org/10.1083/jcb.122.3.729

Doyle, A.D., F.W. Wang, K. Matsumoto, and K.M. Yamada. 2009. One-dimensional topography underlies three-dimensional fibrillar cell migration. *J. Cell Biol.* 184:481–490. http://dx.doi.org/10.1083/jcb.200810041

Even-Ram, S., A.D. Doyle, M.A. Conti, K. Matsumoto, R.S. Adelstein, and K.M. Yamada. 2007. Myosin IIA regulates cell motility and actomyosin-microtubule crosstalk. *Nat. Cell Biol.* 9:299–309. http://dx.doi.org/10.1038/ncb1540

Féral, C.C., D.M. Rose, J. Han, N. Fox, G.J. Silverman, K. Kaushansky, and M.H. Ginsberg. 2006. Blocking the alpha 4 integrin-paxillin interaction selectively impairs mononuclear leukocyte recruitment to an inflammatory site. *J. Clin. Invest.* 116:715–723. http://dx.doi.org/10.1172/JCI26091

Friedl, P., and S. Alexander. 2011. Cancer invasion and the microenvironment: plasticity and reciprocity. *Cell*. 147:992–1009. http://dx.doi.org/10.1016/j.cell.2011.11.016

Garmy-Susini, B., H. Jin, Y. Zhu, R.J. Sung, R. Hwang, and J. Varner. 2005. Integrin alpha4beta1-VCAM-1-mediated adhesion between endothelial and mural cells is required for blood vessel maturation. *J. Clin. Invest.* 115:1542–1551. http://dx.doi.org/10.1172/JCI23445

Ghibaudo, M., L. Trichet, J. Le Digabel, A. Richert, P. Hersen, and B. Ladoux. 2009. Substrate topography induces a crossover from 2D to 3D behavior in fibroblast migration. *Biophys. J.* 97:357–368. http://dx.doi.org/10.1016/j.bpj.2009.04.024

Giannone, G., B.J. Dubin-Thaler, O. Rossier, Y. Cai, O. Chaga, G. Jiang, W. Beaver, H.G. Döbereiner, Y. Freund, G. Borisy, and M.P. Sheetz. 2007. Lamellipodial actin mechanically links myosin activity with adhesion-site formation. *Cell*. 128:561–575. http://dx.doi.org/10.1016/j.cell.2006.12.039

Goldfinger, L.E., J. Han, W.B. Kiosses, A.K. Howe, and M.H. Ginsberg. 2003. Spatial restriction of α4 integrin phosphorylation regulates lamellipodial stability and α4β1-dependent cell migration. *J. Cell Biol.* 162:731–741. http://dx.doi.org/10.1083/jcb.200304031

Grazioli, A., C.S. Alves, K. Konstantopoulos, and J.T. Yang. 2006. Defective blood vessel development and pericyte/pvSMC distribution in alpha 4 integrin-deficient mouse embryos. *Dev. Biol.* 293:165–177. http://dx.doi.org/10.1016/j.ydbio.2006.01.026

Guilluy, C., R. Garcia-Mata, and K. Burridge. 2011. Rho protein crosstalk: another social network? *Trends Cell Biol.* 21:718–726. http://dx.doi.org/10.1016/j.tcb.2011.08.002

Han, J., S. Liu, D.M. Rose, D.D. Schlaepfer, H. McDonald, and M.H. Ginsberg. 2001. Phosphorylation of the integrin alpha 4 cytoplasmic domain regulates paxillin binding. *J. Biol. Chem.* 276:40903–40909. http://dx.doi.org/10.1074/jbc.M102665200

Jacobelli, J., R.S. Friedman, M.A. Conti, A.M. Lennon-Dumenil, M. Piel, C.M. Sorensen, R.S. Adelstein, and M.F. Krummel. 2010. Confinement-optimized three-dimensional T cell amoeboid motility is modulated via myosin IIA-regulated adhesions. *Nat. Immunol.* 11:953–961. http://dx.doi.org/10.1038/ni.1936

Jalali, S., M.A. del Pozo, K. Chen, H. Miao, Y. Li, M.A. Schwartz, J.Y. Shyy, and S. Chien. 2001. Integrin-mediated mechanotransduction requires its dynamic interaction with specific extracellular matrix (ECM) ligands. *Proc. Natl. Acad. Sci. USA*. 98:1042–1046. http://dx.doi.org/10.1073/pnas.98.3.1042

Janmey, P.A., and D.A. Weitz. 2004. Dealing with mechanics: mechanisms of force transduction in cells. *Trends Biochem. Sci.* 29:364–370. http://dx.doi.org/10.1016/j.tibs.2004.05.003

Kelley, C.A., J.R. Sellers, D.L. Gard, D. Bui, R.S. Adelstein, and I.C. Baines. 1996. *Xenopus* nonmuscle myosin heavy chain isoforms have different subcellular localizations and enzymatic activities. *J. Cell Biol.* 134:675–687. http://dx.doi.org/10.1083/jcb.134.3.675

Kil, S.H., C.E. Krull, G. Cann, D. Clegg, and M. Bronner-Fraser. 1998. The alpha4 subunit of integrin is important for neural crest cell migration. *Dev. Biol.* 202:29–42. http://dx.doi.org/10.1006/dbio.1998.8985

Konstantopoulos, K., and L.V. McIntire. 1997. Effects of fluid dynamic forces on vascular cell adhesion. *J. Clin. Invest.* 100(Suppl.):S19–S23..

Konstantopoulos, K., P.H. Wu, and D. Wirtz. 2013. Dimensional control of cancer cell migration. *Biophys. J.* 104:279–280. http://dx.doi.org/10.1016/j.bpj.2012.12.016

Kummer, C., B.G. Petrich, D.M. Rose, and M.H. Ginsberg. 2010. A small molecule that inhibits the interaction of paxillin and alpha 4 integrin inhibits accumulation of mononuclear leukocytes at a site of inflammation. *J. Biol. Chem.* 285:9462–9469. http://dx.doi.org/10.1074/jbc.M109.066993

Leeuwen, F.N., H.E. Kain, R.A. Kammen, F. Michiels, O.W. Kranenburg, and J.G. Collard. 1997. The guanine nucleotide exchange factor Tiam1 affects neuronal morphology; opposing roles for the small GTPases Rac and Rho. *J. Cell Biol.* 139:797–807. http://dx.doi.org/10.1083/jcb.139.3.797

Li, S., P. Butler, Y. Wang, Y. Hu, D.C. Han, S. Usami, J.L. Guan, and S. Chien. 2002. The role of the dynamics of focal adhesion kinase in the mechanotaxis of endothelial cells. *Proc. Natl. Acad. Sci. USA*. 99:3546–3551. http://dx.doi.org/10.1073/pnas.052018099

Liao, J.K., M. Seto, and K. Noma. 2007. Rho kinase (ROCK) inhibitors. *J. Cardiovasc. Pharmacol.* 50:17–24. http://dx.doi.org/10.1097/FJC.0b013e318070d1bd

Lim, C.J., J. Han, N. Yousefi, Y. Ma, P.S. Amieux, G.S. McKnight, S.S. Taylor, and M.H. Ginsberg. 2007. Alpha4 integrins are type I cAMP-dependent protein kinase-anchoring proteins. *Nat. Cell Biol.* 9:415–421. http://dx.doi.org/10.1038/ncb1561

Limouze, J., A.F. Straight, T. Mitchison, and J.R. Sellers. 2004. Specificity of blebbistatin, an inhibitor of myosin II. *J. Muscle Res. Cell Motil.* 25:337–341. http://dx.doi.org/10.1007/s10974-004-6060-7

Liu, S., S.M. Thomas, D.G. Woodside, D.M. Rose, W.B. Kiosses, M. Pfaff, and M.H. Ginsberg. 1999. Binding of paxillin to alpha4 integrins modifies integrin-dependent biological responses. *Nature*. 402:676–681. http://dx.doi.org/10.1038/45264

Matsuura, N., W. Puzon-McLaughlin, A. Irie, Y. Morikawa, K. Kakudo, and Y. Takada. 1996. Induction of experimental bone metastasis in mice by transfection of integrin alpha 4 beta 1 into tumor cells. *Am. J. Pathol.* 148:55–61.

McBeath, R., D.M. Pirone, C.M. Nelson, K. Bhadriraju, and C.S. Chen. 2004. Cell shape, cytoskeletal tension, and RhoA regulate stem cell lineage commitment. *Dev. Cell*. 6:483–495. http://dx.doi.org/10.1016/S1534-5807(04)00075-9

Mostafavi-Pour, Z., J.A. Askari, S.J. Parkinson, P.J. Parker, T.T. Ng, and M.J. Humphries. 2003. Integrin-specific signaling pathways controlling focal adhesion formation and cell migration. *J. Cell Biol.* 161:155–167. http://dx.doi.org/10.1083/jcb.200210176

Moyano, J.V., A. Maqueda, B. Casanova, and A. Garcia-Pardo. 2003. Alpha4beta1 integrin/ligand interaction inhibits alpha5beta1-induced stress fibers and focal adhesions via down-regulation of RhoA and induces melanoma cell migration. *Mol. Biol. Cell*. 14:3699–3715. http://dx.doi.org/10.1091/mbc.E02-10-0667

Nimnual, A.S., L.J. Taylor, and D. Bar-Sagi. 2003. Redox-dependent down-regulation of Rho by Rac. *Nat. Cell Biol.* 5:236–241. http://dx.doi.org/10.1038/ncb938

Nishiya, N., W.B. Kiosses, J. Han, and M.H. Ginsberg. 2005. An alpha4 integrin-paxillin-Arf-GAP complex restricts Rac activation to the leading edge of migrating cells. *Nat. Cell Biol.* 7:343–352. http://dx.doi.org/10.1038/ncb1234

Pasapera, A.M., I.C. Schneider, E. Rericha, D.D. Schlaepfer, and C.M. Waterman. 2010. Myosin II activity regulates vinculin recruitment to focal adhesions through FAK-mediated paxillin phosphorylation. *J. Cell Biol.* 188:877–890. http://dx.doi.org/10.1083/jcb.200906012

Pathak, A., and S. Kumar. 2012. Independent regulation of tumor cell migration by matrix stiffness and confinement. *Proc. Natl. Acad. Sci. USA*. 109:10334–10339. http://dx.doi.org/10.1073/pnas.1118073109

Petrie, R.J., N. Gavara, R.S. Chadwick, and K.M. Yamada. 2012. Nonpolarized signaling reveals two distinct modes of 3D cell migration. *J. Cell Biol.* 197:439–455. http://dx.doi.org/10.1083/jcb.201201124

Pinco, K.A., W. He, and J.T. Yang. 2002. alpha4beta1 integrin regulates lamellipodia protrusion via a focal complex/focal adhesion-independent mechanism. *Mol. Biol. Cell*. 13:3203–3217. http://dx.doi.org/10.1091/mbc.02-05-0086

Ren, Y., J.C. Effler, M. Norstrom, T. Luo, R.A. Firtel, P.A. Iglesias, R.S. Rock, and D.N. Robinson. 2009. Mechanosensing through cooperative interactions between myosin II and the actin crosslinker cortexillin I. *Curr. Biol.* 19:1421–1428. http://dx.doi.org/10.1016/j.cub.2009.07.018

Rivera Rosado, L.A., T.A. Horn, S.C. McGrath, R.J. Cotter, and J.T. Yang. 2011. Association between α4 integrin cytoplasmic tail and non-muscle myosin IIA regulates cell migration. *J. Cell Sci.* 124:483–492. http://dx.doi.org/10.1242/jcs.074211

Roca-Cusachs, P., T. Iskratsch, and M.P. Sheetz. 2012. Finding the weakest link: exploring integrin-mediated mechanical molecular pathways. *J. Cell Sci.* 125:3025–3038. http://dx.doi.org/10.1242/jcs.095794

Ryu, B., D.S. Kim, A.M. Deluca, and R.M. Alani. 2007. Comprehensive expression profiling of tumor cell lines identifies molecular signatures of melanoma progression. *PLoS ONE*. 2:e594. http://dx.doi.org/10.1371/journal.pone.0000594

Sanders, L.C., F. Matsumura, G.M. Bokoch, and P. de Lanerolle. 1999. Inhibition of myosin light chain kinase by p21-activated kinase. *Science*. 283:2083–2085. http://dx.doi.org/10.1126/science.283.5410.2083

Sandquist, J.C., K.I. Swenson, K.A. Demali, K. Burridge, and A.R. Means. 2006. Rho kinase differentially regulates phosphorylation of nonmuscle myosin II isoforms A and B during cell rounding and migration. *J. Biol. Chem.* 281:35873–35883. http://dx.doi.org/10.1074/jbc.M605343200

Sanz-Moreno, V., G. Gadea, J. Ahn, H. Paterson, P. Marra, S. Pinner, E. Sahai, and C.J. Marshall. 2008. Rac activation and inactivation control plasticity of tumor cell movement. *Cell*. 135:510–523. http://dx.doi.org/10.1016/j.cell.2008.09.043

Schwarz, U.S., and M.L. Gardel. 2012. United we stand: integrating the actin cytoskeleton and cell-matrix adhesions in cellular mechanotransduction. *J. Cell Sci.* 125:3051–3060. http://dx.doi.org/10.1242/jcs.093716

Sengbusch, J.K., W. He, K.A. Pinco, and J.T. Yang. 2002. Dual functions of α4β1 integrin in epicardial development: initial migration and long-term attachment. *J. Cell Biol.* 157:873–882. http://dx.doi.org/10.1083/jcb.200203075

Sixt, M. 2012. Cell migration: Fibroblasts find a new way to get ahead. *J. Cell Biol.* 197:347–349. http://dx.doi.org/10.1083/jcb.201204039

Stroka, K.M., and H. Aranda-Espinoza. 2011. Endothelial cell substrate stiffness influences neutrophil transmigration via myosin light chain kinase-dependent cell contraction. *Blood*. 118:1632–1640. http://dx.doi.org/10.1182/blood-2010-11-321125

Stroka, K.M., J.A. Vaitkus, and H. Aranda-Espinoza. 2012. Endothelial cells undergo morphological, biomechanical, and dynamic changes in response to tumor necrosis factor-α. *Eur. Biophys. J.* 41:939–947. http://dx.doi.org/10.1007/s00249-012-0851-3

Tong, Z., E.M. Balzer, M.R. Dallas, W.C. Hung, K.J. Stebe, and K. Konstantopoulos. 2012a. Chemotaxis of cell populations through confined spaces at single-cell resolution. *PLoS ONE*. 7:e29211. http://dx.doi.org/10.1371/journal.pone.0029211

Tong, Z., L.S. Cheung, K.J. Stebe, and K. Konstantopoulos. 2012b. Selectin-mediated adhesion in shear flow using micropatterned substrates: multiple-bond interactions govern the critical length for cell binding. *Integr. Biol. (Camb.)*. 4:847–856. http://dx.doi.org/10.1039/c2ib20036h

Vicente-Manzanares, M., J. Zareno, L. Whitmore, C.K. Choi, and A.F. Horwitz. 2007. Regulation of protrusion, adhesion dynamics, and polarity by myosins IIA and IIB in migrating cells. *J. Cell Biol.* 176:573–580. http://dx.doi.org/10.1083/jcb.200612043

Vicente-Manzanares, M., K. Newell-Litwa, A.I. Bachir, L.A. Whitmore, and A.R. Horwitz. 2011. Myosin IIA/IIB restrict adhesive and protrusive signaling to generate front–back polarity in migrating cells. *J. Cell Biol.* 193:381–396. http://dx.doi.org/10.1083/jcb.201012159

Wolf, K., S. Alexander, V. Schacht, L.M. Coussens, U.H. von Andrian, J. van Rheenen, E. Deryugina, and P. Friedl. 2009. Collagen-based cell migration models in vitro and in vivo. *Semin. Cell Dev. Biol.* 20:931–941. http://dx.doi.org/10.1016/j.semcdb.2009.08.005

Yednock, T.A., C. Cannon, L.C. Fritz, F. Sanchez-Madrid, L. Steinman, and N. Karin. 1992. Prevention of experimental autoimmune encephalomyelitis by antibodies against alpha 4 beta 1 integrin. *Nature*. 356:63–66. http://dx.doi.org/10.1038/356063a0

Yoshida, K., and T. Soldati. 2006. Dissection of amoeboid movement into two mechanically distinct modes. *J. Cell Sci.* 119:3833–3844. http://dx.doi.org/10.1242/jcs.03152